

~~1 Multidimensional mapping of root responses to soil~~

~~2 environmental cues using a luminescence-based GLO-Roots:~~

~~3 an imaging systemplatform enabling multidimensional~~

~~4 characterization of soil-grown roots systems~~

Rubén Rellán-Álvarez^{1, 9}, Guillaume Lobet², Heike Lindner^{1, 8}, Pierre-Luc Pradier^{1, 8, 10},
~~Jose Sebastian^{1, 8}~~, Muh-Ching Yee¹, ~~Jose Sebastian¹~~, Yu Geng^{1, 7}, Charlotte Trontin¹,
Therese LaRue³, Amanda Schrager-Lavelle⁴, Cara ~~H.~~ Haney⁵, Rita Nieu⁶, Julin Maloof⁴,
John P. Vogel⁷, José R. Dinneny^{1, 12}

⁹ ¹ Department of Plant Biology, Carnegie Institution for Science, Stanford, CA, USA.

¹⁰ ² PhytoSystems, University of Liège, Liège, Belgium.

¹¹ ³ Department of Biology, Stanford University, Stanford, CA, USA.

¹² ⁴ Department of Plant Biology, UC Davis, Davis, CA, USA.

¹³ ⁵ Harvard Medical School/Massachusetts General Hospital, Department of Genetics/Department of Molecular Biology Boston, MA, USA

¹⁵ ⁶ USDA Western Regional Research Center, Albany, CA, USA

¹⁶ ⁷ DOE Joint Genome Institute, Walnut Creek, CA, USA

¹⁷ ⁸ These authors contributed equally

¹⁸ ⁹ Present address: ~~Unidad Laboratorio Nacional de Genómica Avanzada para la Biodiversidad~~ (Langebio), ~~CINVESTAV-Irapuato, Unidad de Genómica Avanzada, Centro de Investigación y de Estudios Avanzados del Instituto Politécnico Nacional (CINVESTAV-IPN)~~, Irapuato, GTO, México

²² ¹⁰ Present address: Boyce Thompson Institute for Plant Research/USDA, Ithaca, NY, USA.

²³ ¹¹ Present address: Energy Biosciences Institute, UC, Berkeley, CA, USA

²⁴ ¹² Corresponding author

²⁵ **Author contributions:**

²⁶ RR-A: Conception, design and development of the growth and imaging system and Arabidopsis transgenic lines; acquisition, analysis and interpretation of data; drafting and revising the article.

²⁹ GL: Development of the GLO-RIA image analysis plugin, analysis and interpretation of data, drafting and revising the article.

³¹ HL: Acquisition of data, development of the tomato growth and imaging setup.

³² P-LP: Acquisition of data, analysis and interpretation of data

³³ **MCY: Development of Arabidopsis and Brachypodium transgenic lines.**

³⁴ JS: Development of Brachypodium transgenic lines, acquisition and analysis of Brachypodium [Arabidopsis and tomato](#) data.

³⁶ **MCY: Development of Arabidopsis and Brachypodium transgenic lines.**

³⁷ YG: Development of Arabidopsis transgenic lines.

³⁸ CT: Acquisition and analysis of the QPCR data

³⁹ TL: Acquisition and analysis of the QPCR data

⁴⁰ AS-L: Contributed the unpublished dual-color tomato line.

⁴¹ CH: Contributed the unpublished *Pseudomonas fluorescens* CH267-lux strain.

⁴² RN: Contribution to the development of the Brachypodium transgenic line.

⁴³ JM: Contributed the unpublished dual-color tomato line.

⁴⁴ JPV: Contribution to the development of the Brachypodium transgenic line.

⁴⁵ JRD: Conception, design and development of the growth and imaging system and Arabidopsis transgenic lines; acquisition, analysis and interpretation of data; drafting and revising the article.

⁴⁸ All authors read and approve the final version of the manuscript.

⁴⁹ **Abstract**

⁵⁰ Root systems develop different root types that individually sense cues from their local
⁵¹ environment and integrate them with systemic signals. This complex multi-dimensional
⁵² amalgam of inputs leads to continuous adjustment of root growth rates, direction and
⁵³ metabolic activity to define a dynamic physical network. Current methods for analyzing
⁵⁴ root biology balance physiological relevance with imaging capability. To bridge this divide,
⁵⁵ we developed an integrated imaging system called Growth and Luminescence Observatory
⁵⁶ for Roots (GLO-Roots) that uses luminescence-based reporters to enable studies of root
⁵⁷ architecture and gene expression patterns in soil-grown, light-shielded roots. We have
⁵⁸ developed image analysis algorithms that allow the spatial integration of soil properties
⁵⁹ such as soil moisture with root traits. We propose GLO-Roots as a system that has great
⁶⁰ utility in both presenting environmental stimuli to roots in ways that evoke natural adaptive
⁶¹ responses, and in providing tools for developing a multi-dimensional understanding of such
⁶² processes.

⁶³ **Introduction**

⁶⁴ Plant roots are three-dimensional assemblies of cells that coordinately monitor and acclimate
⁶⁵ to soil environmental change by altering physiological and developmental processes through
⁶⁶ cell-type and organ-specific regulatory mechanisms^{1,2}. Soil comprises a complex distribution
⁶⁷ of particles of different size, composition and physical properties, airspaces, variation in
⁶⁸ nutrient availability and microbial diversity^{3,4}. These physical, chemical and biological
⁶⁹ properties of soil can vary on spatial scales of meters to microns, and on temporal scales
⁷⁰ ranging from seasonal change to seconds. Root tips likely monitor this environment through
⁷¹ locally and systemically acting sensory mechanisms^{5,6}.

⁷² The architecture of the root system determines the volume of soil where resources can be

73 accessed by the plant (rhizosphere). Because the physical and chemical properties of these
74 resources vary, their distribution in the soil column is distinct⁴. Water and water-soluble
75 nutrients such as nitrogen or manganese move through the soil by bulk flow and tend to
76 accumulate deeper in the soil profile as a consequence of gravity⁷, while other nutrients
77 such as phosphorus and potassium, which tightly bind to soil particles, tend to accumulate
78 in the upper layers of soil where decomposition of organic matter replenishes their supply⁷.
79 Developmental processes that affect root growth rate and direction will influence the
80 efficiency with which specific resources are captured from the rhizosphere. Root systems
81 optimized to capture one resource may be inefficient for another.

82 Root architecture is and is under both environmental and genetic control; plasticity.
83 Plasticity in growth parameters allows the plant to adjust its form to suit a particular
84 soil. Lateral roots, which usually make up the majority of the total root system, often
85 grow at an angle divergent from the gravity vector. This gravity set-point angle (GSA) is
86 controlled by auxin biosynthesis and signaling and can be regulated by developmental age
87 and root type⁸⁷. Recent cloning of the *DRO1* Quantitative Trait Locus (QTL) demonstrates
88 that natural genetic variation is a powerful tool for uncovering such control mechanisms⁹⁸.
89 Specific root ideotypes (idealized phenotypes) have been proposed to be optimal for acquisition
90 of water and nitrogen, which are distinct from ideotypes for low phosphorus. Based on
91 computational modeling and field studies, the “steep, deep and cheap” ideotype proposed
92 by Lynch and colleagues may provide advantages to the plant for capturing water and
93 nitrogen elements like nitrogen that are water soluble and therefore tend to move in the soil
94 column with water. This ideotype consists of highly gravitropic, vertically oriented roots
95 that grow deep in the soil column and develop large amounts of aerenchyma, which reduces
96 the overall metabolic cost of the root system³. Low phosphorus conditions, on the other
97 hand, Other elements, like phosphorus that are not water soluble and are tightly bound to
98 organic matter usually accumulate in the top layers of soil favor root systems that are more
99 highly branched and shallow effectively increasing the effective root exploration surface in
100 the top layers of soil³. Modeling of root system variables shows that optimum architecture

101 for nitrogen and phosphorus uptake are not the same¹⁰⁹ and suggests tradeoffs that may
102 affect the evolution of root architecture as a population adapts to a particular environmental
103 niche.

104 Clearly, understanding the architecture of root systems and how environmental conditions
105 alter root developmental programs is important for understanding adaptive mechanisms of plants and for identifying the molecular-genetic basis for different response programs.~~Experimental methods for studying root architecture can be divided into two general categories that each represent compromises in either physiological relevance or versatility.~~

109 ~~Growth of plants in gels such as agar or gellan gum provides a transparent support medium which allows immediate visual access to roots. Simple devices can be used to capture macroscopic images of roots¹¹ or confocal microscopy can be implemented for studying cell-scale processes. Gel media allows exact control over the concentration of nutrients¹² or stressful components¹³ and fluorescent reporters can be deployed to track the activity of genes, proteins or metabolites. This approach has been extensively used in the model plant Arabidopsis and has allowed for the discovery of many fundamental processes. Root system architecture studies and high resolution time-scale analysis of root growth are easily performed when used in combination with automatic time-lapse imaging^{14,15}. Variations of this approach have been used in other species to study root system architecture in three dimensions???. Most often, in gel-based media systems, roots are exposed to light¹⁷ while shoots are enclosed in a high humidity head space that does not permit transpiration from the leaf surface. Media is typically axenic and with highly artificial levels and distributions of nutrients. Gas exchange between the root and the media is limited and might lead to hypoxia or ethylene buildup. *In vitro* growth conditions are also limited in the length of time plant growth can be supported. Typical studies examine roots during the first 1-2 weeks after seed germination whereas the life-cycle of Arabidopsis lasts for two months or longer, depending on the accession. Moreover, the relevance of root architectural phenotypes that are highly influenced by light raises concerns regarding the importance of any loci identified using *in vitro* conditions¹⁷. Due to these limitations, studying processes that involve whole plant~~

129 sensing of environmental cues such as water or nutrient availability must be viewed with
130 caution.

131 A less transparent but more physiologically relevant medium to study root growth is
132 soil. Plants are grown in soil in the field or in pots. Root imaging can be achieved by
133 several means, from uprooting plants using a shoveling pipeline^{18,19} to growth of roots
134 in transparent pots or in rhizotrons²⁰, literally “root devices” that are constructed to
135 allow visualization of roots in proximity to a transparent glass or plastic plate. More
136 recently, the use of techniques such as X-ray micro computed tomography has opened the
137 possibility of *in situ* characterization of root architecture, water content and soil particles
138 in 3-D^{5,21}. Such methods are limited due to their relative cost, the volume of soil that can
139 be imaged, the current limit in resolution and the inability to monitor gene expression or
140 other molecular processes.

141 Roots systems have additional In addition, roots systems have complexity beyond their
142 architecture that needs to be incorporated into our understanding of plant-environment inter-
143 actions. Primary and lateral roots exhibit different stress response programs in *Arabidopsis*²
144 and may play specialized roles in water and nutrient uptake. Thus, it is important to
145 develop methods that allow for a multidimensional characterization of the root system that
146 includes growth, signaling, and interactions with other organisms. Furthermore, physiological
147 parameters that affect whole plant responses to the environment, such as transpiration, are
148 likely integrated into such processes, thus requiring a more holistic approach to studies of
149 root function.

150 Based on these considerations we have developed a new root imaging platform, Growth and
151 Luminescence Observatory for Roots (GLO-Roots), which allows root architecture and gene
152 expression to be studied in soil-grown plants. GLO-Roots is an integrated system composed
153 of custom growth vessels, luminescent reporters and imaging systems. We use rhizotrons
154 that have soil volumes equivalent to small pots and support growth of *Arabidopsis* from
155 germination to senescence. To visualize roots, we designed plant-codon optimized luciferase
156 reporters that emit light of different wavelengths. To visualize reporter expression, plants

157 are watered with a dilute luciferin solution and imaged afterwards. We have ~~designed~~built
158 a custom luminescence imaging system that automatically captures images of rhizotrons
159 held vertically. The signal from each reporter is distinguished using band-pass filters held
160 in a motorized filter wheel, which enables automated acquisition of images from plants
161 expressing both structural and environmentally and developmentally responsive reporters.
162 We have also developed GLO-RIA (GLO-Roots Image Analysis) ~~software~~, an ImageJ???
163 plugin that allows for automated determination of root system area, convex hull, depth,
164 width and directionality, which quantifies the angle of root segments with respect to gravity.
165 GLO-RIA is also able to relate root system parameters to local root-associated variables
166 such as reporter expression intensity or soil-moisture content.
167 Overall GLO-Roots has great utility in presenting environmental stimuli to roots in physi-
168 logically relevant ways and provides tools for characterizing responses to such stimuli at
169 the molecular level ~~whole roots of adult plants~~of whole adult root systems over broad time
170 scales.

171 **Box 1.**

172 All resources for GLO-Roots, including the user manual, the latest software downloads, the
173 source code, the original raw data used in the manuscript and sample images can be found
174 on https://github.com/rr-lab/glo_roots.

175 **Results**

176 We have developed an integrated platform for growing, imaging and analyzing root growth
177 that provides advances in physiological relevance and retains the ability to visualize aspects
178 of root biology beyond structure.

179 **THE GLO-ROOTS PLATFORM**The GLO-Roots platform

180 GLO-Roots is comprised of four parts: i) growth vessels called rhizotrons that allow plant
181 growth in soil and root imaging; ii) luminescent reporters that allow various aspects of
182 root biology to be tracked in living plants; iii) luminescence imaging system designed to
183 automatically image rhizotrons; iv) GLO-RIA, an image analysis suite designed to quantify
184 root systems imaged using GLO-Roots.

185 **Plant growth system** GLO-Roots utilizes custom designed growth vessels classically
186 known as rhizotrons, which hold a thin volume of soil between two sheets of polycarbonate
187 plastic. Acrylic spacers provide a 2-mm space in which standard peat-based potting mix is
188 added. Black vinyl sheets protect roots from light and rubber U-channels clamp the rhizotron
189 materials together. Plastic racks hold the rhizotrons vertically and further protect the roots
190 from light. Rhizotrons and rack are placed in a black tub and about 2 cm of water are
191 addedto, to a depth of about 2 cm, at the bottom to maintain moisture in the rhizotrons
192 during plant growth. The volume of soil in the rhizotrons (100 cm^3) is similar to small pots
193 commonly used for *Arabidopsis* growth and supports growth of *Arabidopsis* throughout its
194 throughout the entire life cycle (Fig 1A-C and Supplement 1).

195 While the 2 mm depth of the soil sheet is 20 times the average diameter of the *Arabidopsis*
196 root tip (approximately 100 microns), we wanted to evaluate whether rhizotron-grown plants
197 exhibited any obvious stress as a consequence of physical constriction. We compared traits
198 of plants growing in vessels that hold similar volumes of soil but in different geometric
199 shapes. No significant differences in shoot area were observed between the three systems
200 (not shown). The number of lateral roots was significantly lower in pot and cylinder-grown
201 plants compared to rhizotron-grown plants (Fig 1F) whereas primary root length of rhizotron
202 and cylinder-grown plants was similar and significantly greater than for pot-grown plants
203 (Fig 1G). Thus, these data do not support the hypothesis that rhizotron-grown plants
204 experience physical constriction greater than other vessels holding the same volume of soil.

205

206 We next compared root systems grown on the surface of agar or in soil. Shoot weight
207 and primary root length were significantly reduced for gel-grown plants compared to
208 rhizotron- or pot-grown plants suggesting significant differences in the biology of plants
209 grown under these conditions (Fig 1H-I). To determine how soil-grown and gel-grown
210 root systems might differ in their biology To determine how the biology of plants grown
211 in rhizotrons compares to other standard growth systems, we utilized high-throughput
212 qRT-PCR to study a panel how these conditions affect expression of 77 genes marker
213 genes in root and shoot samples. These genes were curated from the literature that
214 and belong to a wide array of biological pathways including nutrient acquisition and
215 hormone and light response to and abiotic stress. Whole roots and shoot samples were
216 collected at the end of the light and dark cycles (16 hour light, 8 hours dark) from plants
217 grown in rhizotrons, pots, and petri dishes with two different media recipes compositions
218 (1X MS Murashige and Skoog basal salts (MS), 1% sucrose or 0.25X MS, no sucrose).
219 Principal component analysis of the gene expression values showed a clear separation of
220 soil and gel-grown root systems in the first two principal components with a clear overlap
221 between rhizotron and pot-grown root system samples (Fig 1D). Significant differences in
222 the first principal components (Figure 1-figure supplement 1A). We observed enhanced
223 expression of genes associated with flavonoid biosynthesis (light-regulated pathways
224 (flavonoid biosynthesis: *FLAVINOL SYNTHASE1*, *FLS1*) and phosphorus nutrition
225 (*LOW PHOSPHATE RESPONSE1*, *LPR1**CHALCONE SYNTHASE*, *PHOSPHATE
STARVATION RESPONSE1*, *PHR1**CHS*) were observed (Fig 1E) Flavonoids contribute
227 to anthocyanin biosynthesis, which are UV protectants. Importantly, however, flavonoids
228 have also been implicated in the regulation of root developmental traits²², suggesting that
229 light-induction of these pathways in (photosynthesis: *RUBISCO SUBUNITS1A*, *RBCS1A*
230 *CYCLOPHILIN 38*, *CYP38*), which is expected due to the exposure of gel-grown roots
231 could influence such processes. *SUPER ROOT1 (SUR1)*, which promotes biosynthesis of the
232 anti-microbial metabolite indole glucosinolate, was significantly associated with soil-grown
233 roots, suggesting the non-sterile soil environment may induce to light. In addition, genes as-
234 sociated with defense. *XYLOGLUCAN ENDOTRANSGLUCOSYLASE/HYDROLASE17*

(*XTH17*) and *TOUCH4* (*TCH4*), both of which respond to touch stimuli, were expressed more highly. *LOW PHOSPHATE RESPONSE1*, *LPR1*, *PHOSPHATE STARVATION RESPONSE1*, *PHR1* were among others (Figure 1-figure table supplement 1) expressed predominantly in soil-grown roots, consistent with the presence of physical barriers in soil while growth in gel may present fewer obstructions. suggesting differences in nutrient availability between the different growth systems.

Interestingly, shoot samples were not clearly distinguished by growth media and, instead, time of day had a greater effect (Fig. 1E and Figure 1-Supplement 1Figure 1-Supplement 2). These data suggest root systems may be particularly sensitive to media conditions and indicate that rhizotron-grown root systems more closely approximate the biology of a pot-grown plant than standard gel-based media. Shoot weight and primary root length were significantly reduced for gel-grown plants compared to rhizotron- or pot-grown plants suggesting significant differences in the biology of plants grown under these conditions (Figure 1-figure supplement 1B-C). While the 2 mm depth of the soil sheet is 10 to 20 times the average diameter of an *Arabidopsis* root (between 100-200 microns), we evaluated whether rhizotron-grown plants exhibited any obvious stress as a consequence of physical constriction. We compared traits of plants growing in vessels that hold similar volumes of soil but in different volumetric shapes. The number of lateral roots was significantly lower in pot and cylinder-grown plants compared to rhizotron-grown plants (Figure 1-figure supplement 1D) whereas primary root length of rhizotron and cylinder-grown plants was significantly greater than pot-grown plants (Figure 1-figure supplement 1E). No significant differences in shoot area were observed between the three systems (Figure 1-figure supplement 1-data). Thus, these data do not support the hypothesis that rhizotron-grown plants experience physical constriction greater than other vessels holding the same volume of soil.

Generation of transgenic plants expressing different luciferases *Arabidopsis* roots cannot be easily distinguished from soil using brightfield imaging due to their thinness and translucency (Figure 1-figure supplement 3); thus, reporter genes are needed to

enhance the contrast between the root and their environment. Luciferase is an ideal reporter to visualize roots: 1) unlike fluorescent reporters, luciferase does not require high-intensity excitation light, which could influence root growth, 2) peat-based soil ([a type of histosol](#)) exhibits no autoluminescence but does autofluoresce at certain excitation wavelengths similar to GFP ([data not shown](#)[Figure 1-figure supplement 3](#)), 3) while GFP is very stable, and thus not as suitable for imaging dynamic transcriptional events, the luciferase enzyme is inactivated after catabolism of luciferin, making it ideal for studying processes such as environmental responses. A considerable number of luciferases have been developed that emit light spanning different regions of the visible spectrum, but their utilization has been limited to studies in animals (Table 1).

To determine the efficacy of using luciferase to visualize roots in soil, we codon optimized sequences of *PpyRe8PpyRE8*, *CBGRed*, *LUC2*, and *CBG99* for Arabidopsis expression. In addition, nanoLUC and venus-LUC2²³¹⁰ were utilized. Constitutive luciferase expression was driven in plants using the *UBQUITIN 10* (*UBQ10*) or *ACTIN2* (*ACT2*) promoter using vectors assembled through a [Golden-Gate cloning system](#)[Golden-Gate cloning system](#)²⁴¹¹. Plants homozygous for a single locus T-DNA insertion were evaluated for in vivo emission spectra and luminescence intensity (Fig [2A1D](#)). All the evaluated luciferases use D-luciferin as a substrate facilitating the simultaneous imaging of different luciferases except nanoLUC, which uses a [proprietary substrate](#)[proprietary substrate furimazine](#). In general, luciferases with red-shifted emission spectra were less intense than the green-shifted luciferases (Fig [2A1D](#)). LUC2o showed an emission maximum at 580 nm and a minor peak at 620 nm while CBG99o lacks the minor peak.

GLO1: a semi-automated luminescence imaging system for rhizotrons Luminescence imaging systems commercially available for biomedical research are usually optimized for imaging horizontally held specimens or samples in microtiter plates. Placing rhizotrons in this position would induce a gravitropic response in plants. Working with Bioimaging Solutions (San Diego, CA) we designed and built a luminescence imaging system optimized for rhizotron-grown plants. GLO1 (Growth and Luminescence Observatory 1) uses two

291 back-thinned CCD cameras (Princeton Instruments, USA) to capture partially-overlapping
292 images of rhizotrons while a motorized stage automatically rotates the rhizotron to capture
293 images of both sides (Fig 2B1E). A composite image is generated from the images of each
294 side; Fig 2C1F shows that approximately half of the root system is revealed on each side
295 with few roots being visible on both sides. ~~This result suggests that the depth of soil in~~
296 ~~the rhizotron is sufficient to block visibility of roots beyond the mid point of the soil sheet~~
297 ~~but not so thick that a continuous root system is difficult to reconstruct~~ Apparently, the
298 soil sheet is thick enough to block portions of the root system but thin enough to ensure
299 its continuous structure can be compiled from opposite face views. We tested the ability
300 of GLO1-generated images to reveal complete root systems by manually quantifying the
301 number of lateral roots in excavated root systems of 8 different plants and testing these
302 results against estimates of lateral root number from images of the same plants visually
303 inspected by 4 different persons. These comparisons revealed good correlation ($(R^2 = 0.974)$)
304 between actual lateral root counts and image-based estimation, indicating GLO1-generated
305 root images provide an accurate representation of the in soil-soil root system.

306 Continuous addition of luciferin did not have any significant effect on shoot weight or
307 primary root length (Figure 2-Supplement 1-figure supplement 4). After luciferin addition,
308 luminescence signal could be reliably detected in root systems for up to 10 days, depending
309 on the developmental state of the plant.

310 **GLO-RIA: GLO-Roots Image Analysis** Current image analysis algorithms are
311 optimized for roots that are continuously visible, since they are designed to work with
312 images of roots grown in transparent media or on paper. Root systems visualized with
313 GLO-Roots, however, often contain breaks in the continuity of primary and lateral root
314 signal, which likely results from soil particles obscuring the object. We developed a set of
315 image analysis algorithms that were well suited for the complex root systems ~~which that~~
316 GLO-Roots is able to capture. GLO-RIA (Growth and Luminescence Observatory Root
317 Image Analysis) is an ImageJ plugin ~~that can automatically identify the perimeter of the~~
318 root divided in two modules. The first module (RootSystem) performs four different types

of analysis: i) a local analysis that detects all root particles in the image and computes their position, length and direction; ii) the global analysis performs a root system level analysis and computes the total visible surface, convex hull, width and depth; iii) the shape analysis uses Elliptic Fourier Descriptors or pseudo-landmarks similarly to RootScape^{??} to perform a shape analysis on the root system iv) the directionality analysis computes the mean direction of root particles in a root system (either on the full image or by user-defined region of interest in the image). These four analysis methods are fully automated by default, but can be manually adjusted if needed. The second module of GLO-RIA (RootReporter) was specifically designed for the analysis of multi-layered images such as combinations of gene reporter, root structure and soil moisture. Shortly, the plugin works as follow: i) detection of the gene reporters and the structure reporters in their respective images; ii) if needed, a manual correction can be performed to correct the automated detection; iii) gene reporters are linked with the soil water content and the structure reporters, based on their proximity; iv) gene reporter intensity (either absolute or normalized using the structural reporter) is computed; v) all data are exported and saved to a RSML datafile¹². Gene and structure reporters can be followed across different time and space points. Using an object oriented approach, great care has been taken to facilitate the user interactions on the different images to streamline the analysis process. Table 2 shows a list of root system and quantify aspects of root system geometry derived from this outline. We have also used a that utilizes a sobel filter to identify edges in an imageand quantifies the proportion of quadrants that exhibit a bias in angle of such edges with respect to the axes of the image. Similar algorithms have been used to quantify dynamic changes in the plant cytoskeleton²⁵. Directionality measurements can rapidly capture lateral root angles at the whole root system level without the need to define individual rootsfeatures extracted using GLO-RIA. GLO-RIA does not currently have the ability to reconstruct the root architecture in itself (topological links between roots). This is a challenge for analyzing images captured by GLO-Roots since soil particles cause disruption of root segments.

346 Continuous imaging of root growth

347 The size of our rhizotrons enables undisturbed root system development (before roots reach
348 the sides or the bottom of the rhizotron) for about 21-23 days for the Col-0 accession
349 growing under long day conditions ([Figure 2](#)); however root traits ~~besides width and depth~~
350 ~~can continue to such as directionality can be observed until senescence of the plant later~~
351 ~~stages of plant development. See 35 DAS root system and directionality in Figure 2A-B.~~ An
352 example of a time series spanning 11 to 21 days after sowing (DAS) of Col-0 roots expressing
353 *ProUBQ10:LUC2o* is shown in Fig [3A-2A](#) and [Video 1](#) with a color-coded time projection
354 shown in Fig [3B2C](#). Directionality analysis ([Fig 3E2B](#)) shows a progressive change in root
355 system angles from 0 ° (vertical) to 45 ° as lateral roots take over as the predominant
356 root type. Figure [3D-2D](#) shows the evolution over time of several root traits that can be
357 automatically captured by GLO-RIA (depth, width, area) and others that can be manually
358 quantified (primary root growth rate or number of lateral roots per primary root[length](#)).

359 Root system architecture of different *Arabidopsis* accessions.

360 The study of natural variation for root system architecture and root traits is a powerful
361 approach for understanding adaptive strategies plants use to cope with environmental change
362 and for identifying the genetic basis for such differences. In *Arabidopsis*, Quantitative Trait
363 Locus (QTL) and Genome-Wide Association Studies (GWAS) have led to the identification
364 of genes affecting root development^{[26???](#)}. However, traits are usually measured in seedlings
365 less than 2 week old. Selective pressures that affect allele frequencies in a population likely
366 act on genes that affect root system traits at later stages of the plant life cycle, as well. As
367 a proof of concept to estimate the utility of our root imaging system to phenotype adult
368 root system traits, we transformed a small set of accessions ([Bay-0, Col-0 and Sha](#)) with
369 the *ProUBQ10:LUC2o* reporter and quantified RSA at 22 DAS (~~days after sowing~~[Fig 3A-C](#)).
370 GLO-RIA analysis of these root systems identified several root traits that distinguish Col-0,
371 Bay-0 and Sha([Fig 4](#). [Directionality analysis revealed an abundance of steep-angle regions](#)
372 [in the root system of Bay while Sha showed an abundance of shallow-angled regions and](#)

373 Col-0 was intermediate (Fig 3D). Bay-0 shows the deepest and narrowest root system leading
374 to the highest depth/width ratio while Sha has the widest root system. —Directionality
375 analysis revealed an abundance of steep angle regions in the root system of Bay while Sha
376 showed an abundance of shallow angled regions and Col-0 was intermediate (Fig 4D(Fig
377 3E). Other root traits such as root system area and the vertical center of mass also showed
378 significant differences (Figure 3-figure supplement 1B). Broad sense heritability values for
379 depth (96.3), area (92.0), depth/width (97.8), width (95.7) and vertical center of mass (95.0)
380 were all higher than 90%. —To capture the richness of root architecture shape, we used
381 GLO-RIA to extract pseudo-landmarks describing the shape the root system to perform
382 PCA analysis. The first principal component separates Col-0 and Sha plants from Bay-0
383 ones capturing root systems that vary in the distribution of widths along the vertical axis.
384 (Fig 3F). While Bay-0 shows an homogenous distribution of widths along the vertical axis,
385 Sha and Col-0 are much wider at the top than in the bottom. PC2 seems to be capturing a
386 relationship between width at the top and depth, slightly separating Sha root systems which
387 are wide at the top and deep from Col-0 root systems which are wide but not as deep as in
388 Sha. Using shape information extracted from EFDs we can distinguish the three different
389 accessions using PCA analysis (Fig 3G).

390 GLO-Roots for Brachypodium and Tomato

391 To examine the general applicability of the GLO-Roots system for other species, we introduced
392 LUC2o-expressing reporters into the model grass *Brachypodium distachyon* and the crop
393 plant *Lycopersicon esculentum* (tomato). Brachypodium is well suited to the GLO-Root
394 system because, like Arabidopsis, its small size allows mature root systems to be studied in
395 relatively small soil volumes^{2713,2814}. LUC2o driven by the *ZmUb1* promoter was introduced
396 into Brachypodium using the pANIC vector²⁹¹⁵. Brachypodium roots showed a distinct
397 architecture from Arabidopsis marked by prolific development of secondary and tertiary
398 lateral roots (Fig 5A4A). This is consistent with other studies that show that Brachypodium
399 has a typical grass root system²⁸¹⁴. After 26–28 days of growth, shoot-derived crown roots

400 initiated and took over as the predominant part of the root system (not shown). Comparison
401 of root system development in rhizotrons with gel-based media showed that primary and
402 lateral root growth is more extensive in soil (Fig 5B). Interestingly, previous higher in soil
403 than in plates (Figure 4-figure supplement 1). Previous work has suggested that auxin
404 levels in Brachypodium roots is supra-optimal for growth sub-optimal for growth³⁰¹⁶. Our
405 results suggest that gel based systems may lead to an imbalance in hormone signaling that
406 causes slower growth Pacheco-Villalobos and colleagues suggest that, in Brachypodium, and
407 contrary to what happens in Arabidopsis, ethylene represses *YUCCA* reducing the synthesis
408 of auxin. The reduced growth that we observe in plates and the high levels of ethylene that
409 build up in sealed plates¹⁷ would support this mechanism.

410 Tomato plants were transformed with *Pro35S:PPyRE8o* and *ProeDR5rev:LUC2* reporters.
411 The plants showed more rapid growth than Arabidopsis or Brachypodium and required
412 fertilizer to prevent obvious signs of stress (reduced growth, anthocyanin accumulation).
413 Root systems were imaged from 14 17 DAS plants. Roots showed less branching than for
414 Arabidopsis but showed Arabidopsis but many presumptive lateral root primordia marked
415 by DR5-expression (Fig 5C-D4C-D). These results show that the GLO-Roots method is
416 widely applicable can be applied to study root systems of plants and will likely be useful for
417 studying root systems of other small to medium sized model and plants and for early stages
418 of larger crop plants.

419 Spectrally distinct luciferases enable gene expression patterns, characterization
420 of root system interactions , and microbial colonization and gene expression
421 patterns.

422 Although root system architecture is usually studied in isolated plants, this is rarely the
423 ease in nature where plants compete for soil resources through root-root interactions.
424 Recent work in this area has suggested that roots from the same cultivar can grow without
425 competition while roots from different cultivars avoid each other³¹. One of the major
426 challenges in such studies is the ability to distinguish two overlapping root systems. We We

427 tested whether spectrally distinct luciferase reporters would enable additional information
428 besides root architecture to be captured from root systems. Luciferase reporters have been
429 commonly used to study gene expression and these resources can potentially be utilized to
430 study these regulatory events in soil-grown roots. We transformed *ProACT2:PpyRE8o* into
431 two well studied LUC reporter lines: the auxin response reporter line *ProDR5:LUC¹⁸*
432 (Figure 5A-B) and the Reactive Oxygen Species (ROS) response reporter *ProZAT12:LUC¹⁹*
433 (Figure 5C-D). We implemented in GLO-RIA an algorithm that semi-automatically
434 identifies gene reporter signal and associates this object to the corresponding root structure
435 segment. A graphical representation of the results obtained with Root Reporter can be
436 observed in Figure 5E. Reporter intensity values along the first 5 mm of root tips can also
437 be observed in Figure 5-figure supplement 1. We then took advantage of our ability to
438 constitutively express two spectrally different luciferases and imaged the overlapping root
439 systems ~~of two Col-0 plants~~ (one expressing *ProUBQ10:LUC2o* and the other *ProACT2:Ppy*
440 *RE8o*)~~or one Col-0 plant (expressing ProACT2:Ppy RE8o)~~ and one Sha plant (expressing
441 *ProUBQ10:LUC2o*). Images were captured using unfiltered light and a custom (76.5 mm
442 diameter) band-pass filter (415 nm – 485 nm), which captured light emitted predominantly
443 by LUC2o. By overlaying the images, we were able to distinguish the two overlapping
444 root systems (Figure 6 Supplement 1). We compared root traits of plants grown together
445 or in isolation but could not observe any significant differences between treatments. This
446 was also observed when Col-0 was grown with the Sha accession. Further studies are
447 warranted, however, as environmental conditions where resources are limited may lead to
448 more competition.

449 . Root systems were distinguishable using this system (Figure 5-figure supplement 2);
450 measurements of root system area did not reveal a significant effect on root growth when
451 two plants were grown in the same rhizotron, however further studies are warranted (Figure
452 5-figure supplement 2) The GLO-Roots system uses non-sterile growth conditions, which
453 allows complex biotic interactions that may affect responses to the environment. Bacteria
454 themselves can be engineered to express luminescent reporters through integration of
455 the LUX operon, which results in luminescence in the blue region of the spectrum and is

456 thus compatible with the plant-expressed luciferase isoforms we have tested. *Pseudomonas*
457 *fluorescens* CH267³²²⁰, a natural *Arabidopsis* root commensal, was transformed with the
458 bacterial LUX operon and used to inoculate plants. Thirteen days after inoculation we were
459 able to observe bacterial luminescence colocalizing with plant roots. *P. fluorescens* did not
460 show an obvious pattern of colonization at the root system scale level. As a proof-of-principle
461 test of the multi-dimensional capabilities of the GLO-Roots system we visualized both *LUC2o*
462 and *PPyRE8o* reporters in plants and the LUX reporter in bacteria in the same rhizotron
463 (Figure 65-figure supplement 3).

464 One of the major advantages of our system is that luciferase reporters have been commonly
465 used to study gene expression and these resources can potentially be utilized to study these
466 regulatory events in soil-grown roots. We transformed *ProACT2:PpyRE8o* into two well
467 studied LUC reporter lines: the auxin activity reporter line *ProDR5:LUC*³³ (Figure 7A)
468 and the ROS activity reporter *ProZAT12:LUC*³⁴ (Figure 7B). We implemented in GLO-RIA
469 an algorithm that semi-automatically identifies gene reporter signal and associates this
470 object to the corresponding root structure segment. These two associated variables can
471 be tracked in time lapse experiments. Using the *ProACT2:PpyRE8o* and *ZAT12:LUC* line
472 we tracked root tip associated changes in growth and reporter expression throughout the
473 whole root system in response to a local application of a 1 M NaCl solution over 24 hours. As
474 shown in , reporter activity declines rapidly at the site of salt application while growth and
475 ZAT12 reporter activity become induced further away at later time points and correlates
476 with a burst of growth in this part of the root system (Fig 7E-F).

477 Adaptive changes in root system architecture under water deprivation,
478 phosphorus deficiency and light

479 **ADAPTIVE RESPONSES TO SOIL-BASED ENVIRONMENTAL STIMULI**

480 Phosphorus availability promotes shallow root systems To examine To test the
481 utility of the GLO-Roots system to understand response of root systems to environmental

482 stimuli we tested the effects of phosphorus availability on RSA we used alumina particles
483 buffered with 100 μ M phosphate (P) to supply this macro-nutrient to the root. Alumina
484 particles bind and release inorganic phosphorus similarly to soil particles, thus providing a
485 physiologically relevant nutrient regime³⁵. Alumina particles lacking P, which would remove
486 P supplied by the peat-based soil, were used to simulate a P-deficient soil. Root and shoot
487 phenotypes of control and P-deficient plants at 22 (Fig 8A) and 27 (Fig 8B) DAS are shown.
488 Plants grown in low P soil showed a significant increase in the width-depth ratio of the root
489 system compared to plants grown in P-replete soil, as determined using the automated root
490 system area finder in GLO-RIA (Fig 8). Plants under P deficiency showed an increase in
491 the ratio between root-shoot area (Figure 8C) and higher investment of resources in the
492 development of the root system at the expense of shoot growth (Figure 8D). Root systems
493 of control and P-deficient plants showed no significant differences in directionality at 22
494 DAS but at 27 DAS, roots were more horizontally oriented in P-deficient plants (Figure 8E).
495 The observed changes in root architecture are consistent with root system ideotypes that
496 improve phosphorus uptake efficiency.

497 **Light promotes root gravitropism through PHOTOTROPIN signaling** light and
498 conditions that mimic drought and nutritional deficiency. To examine the effects of light
499 exposure on the root system architecture, the black shields, which normally protect the
500 soil and roots from light, were removed from the top half of the rhizotron 10
501 DAS. Using directionality analysis we detected a significant increase in the steepness of
502 roots only in the light exposed region of the rhizotron, while the lower shielded region
503 showed no difference. (Fig 9A-B^{7-figure supplement 3A-B} and Fig 7^{figure supplement 4}).
504 Light can penetrate the top layers of soil^{36,21} and it has been proposed to have a role in
505 directing root growth (Figure 9 supplement 1) specially in dry soils^{37,22} through the
506 blue light receptor *phot1*. Root directionality was not significantly different between light
507 and dark-treated roots of the *phot1/2* double mutant suggesting that blue light perception is
508 necessary for this response (Fig 9B), which is consistent with previous studies^{37,38,22,23} (Fig
509 7^{figure supplement 3B-lower panel}). These data highlight the strong effects of light on root

510 system architecture¹⁷²⁴, which GLO-Roots rhizotrons are able to mitigate.

511 **Adaptive changes in root system architecture under water deprivation.** Plants
512 grown in low-P soil showed a significant increase in the width-depth ratio of the root
513 system compared to plants grown in P-replete soil, as determined using the automated
514 root system area finder in GLO-RIA (Fig 7-figure supplement 2A-B). Plants under P
515 deficiency showed an increase in the ratio between root-shoot area (Fig 7-figure supplement
516 2C) and higher investment of resources in the development of the root system at the expense
517 of shoot growth (Fig 7-figure supplement 2D). Root systems of control and P-deficient
518 plants showed no significant differences in directionality at 22 DAS but at 27 DAS, roots
519 were more horizontally oriented in P-deficient plants (Fig 7-figure supplement 2E). The
520 observed changes in root architecture are consistent with root system ideotypes that improve
521 phosphorus uptake efficiency.

522 GLO-Roots provides important advantages over gel-based systems is especially well suited
523 for studying water-deficit (WD) responses. First, shoots are exposed to the atmosphere and
524 vapor pressure deficit (VPD) is maintained at levels that allow for transpiration of water
525 from the shoot. Second, WD can be simulated in more realistic ways than in gel. Soil in soil
526 in rhizotrons is exposed to air at the top and dries basipetally (from the top-down); drying
527 soil increases the volume occupied by air and reduces contact of root with liquid water, all of
528 which are similar to changes in soil expected in the field during WD. Finally, as peat-based
529 soil dries, its optical properties change, allowing moisture content to be approximated from
530 bright-field images. We took advantage of the change in gray-scale pixel intensity to construct
531 a calibration curve (Figure 10-Supplement 6-figure supplement 1) that quantitatively relates
532 gray-scale pixel intensity to moisture content (Fig 10A6A); water content can be color coded
533 in images with appropriate look up tables (Fig 10B-6B). Soil color was not affected by
534 the presence or absence of roots (Figure 6-figure supplement 2). Using this approach, water
535 content in a rhizotron can be mapped and visualized in 2D (Fig 10C-D)6C-D). In the example
536 shown, we can observe that a 22 DAS Bay-0 plant depleted soil-moisture content locally
537 around the the root system (Figure 10E6E).

538 We performed several trials to simulate WD in our growth system. Plants were germinated,
539 grown under control conditions then transferred to 29°C and standing water ~~was~~ removed from
540 the container holding the rhizotrons starting at either 9 DAS or 13 DAS. Elevated temperature
541 combined with water deficit is a common stress that modern crops varieties are poorly adapted
542 to, thus highlighting the importance of examining this combined treatment^{3925,4026}. Plants
543 were maintained in this WD regime until 22 DAS when luciferin was added and the plants
544 were imaged. At 13 DAS, lateral roots near the soil surface are already emerged (Video 1,
545 Figure 3A2A). After 9 days of water deficit treatment, lateral roots showed an increase in
546 gravitropism leading to the development of a root system that was deeper, more vertically
547 oriented and with more tertiary roots (Fig 11A7A). Roots of Bay-0 plants showed similar
548 responses though the extent of change was less pronounced since Bay-0 roots are normally
549 more vertically oriented (Fig 11B7B). Plants transferred at 9 DAS showed less lateral
550 root development in the top layer of soil (Fig 11E7E). At this time point, lateral roots
551 start to emerge (Video 1) and early drought may lead to growth quiescence or senescence.
552 Careful examination of roots in these regions showed evidence of small lateral root primordia
553 populating the primary root (Figure 7F). After 24 h of re-watering (Figure 7G) these lateral
554 root primordia reinitiated growth (Figure 7H).

555 Time-lapse imaging of the water deficit response showed that changes in root growth
556 direction occurred ahead of the dry soil front Video 3. Using GLO-RIA we were able
557 correlate water moisture contents with local orientation of the root segments. With this
558 approach we observed that root segments in dryer areas of rhizotron grew at steeper root
559 angles (Figure 8) than roots in growing in well watered regions, though lateral root angle
560 in wetter regions was also affected. These data suggest that local and systemic signaling is
561 likely involved in redirecting lateral roots deeper during the simulated drought treatments
562 tested here.

563 We also grew plants under WD at control temperatures or under WW conditions at ~~high~~
564 ~~elevated~~ temperature to test the effects ~~water and temperature had of these individual~~
565 ~~stresses~~ on root architecture~~in isolation~~. We observed that both conditions were sufficient to

566 induce a change in root directionality indicating that the plant uses similar mechanisms to
567 avoid heat and water-deficit associated stresses (Figure 11~~Supplement~~⁷-figure supplement
568 1). We next asked which regulatory pathways controlled the observed changes in lateral root
569 directionality during simulated drought. Hydrotropism is a known environmental response
570 that directs root growth towards wet regions of soil. MIZ1 is an essential regulator of
571 hydrotropism; however *miz1* mutants had no significant effect on water deficit-induced
572 changes in root directionality, compared to wild type (Fig 11C~~7C~~), indicating that this
573 response was distinct from hydrotropism. Auxin is an important mediator of gravitropism
574 and auxin treatment causes lateral roots to grow more vertically⁸⁷. Consistent with this
575 role for auxin, mutant plants with loss of function in the auxin receptor TIR1, did not show
576 changes in the root system directionality between WW and WD conditions (Fig 11D~~7D~~).

577 ~~Plants transferred at 9 DAS showed less lateral root development in the top layer of soil. (Fig~~
578 ~~11E) At this time point, lateral roots start to emerge (See) and early drought may lead~~
579 ~~to growth quiescence or senescence². Careful examination of roots in these regions showed~~
580 ~~evidence of small lateral root primordia populating parent roots (Figure 11F). After 24 h of~~
581 ~~re-watering (Figure 11G) these lateral root primordia reinitiated growth (Figure 11H)~~
582 ~~Time-lapse imaging of the water deficit response showed that changes in root growth~~
583 ~~direction occurred ahead of the dry soil front. Using GLO-RIA we were able correlate~~
584 ~~water moisture contents with local orientation of the root segments. With this approach~~
585 ~~we observed that root segments in dryer areas of rhizotron grew at steeper root angles~~
586 ~~(Figure 12) than roots in growing in well watered regions, though lateral root angle in~~
587 ~~wetter regions was also affected. These data suggest that local and systemic signaling is~~
588 ~~likely involved in redirecting lateral roots deeper during the simulated drought treatments~~
589 ~~tested here.~~

590 Discussion

591 ~~Organisms have evolved to acclimate to environmental change through adaptive responses.~~
592 ~~Stressful environmental conditions can elicit tolerance mechanisms that allow the organism~~

593 ~~to bear the negative effects of sub-optimal conditions while avoidance mechanisms provide~~
594 ~~alternative routes for acquiring needed resources. Environmental stresses such as phosphate~~
595 ~~deprivation or water deficit simulated in gel-based systems typically cause a reduction in root~~
596 ~~growth, suggesting that the plant is preserving resources to ensure survival. Interestingly,~~
597 ~~simulation of these same stresses using the soil-based GLO-Roots system was able to elicit~~
598 ~~changes in root growth that are anticipated to provide a mechanism to avoid stress. These~~
599 ~~data support the utility of GLO Roots for characterizing environmental responses that are~~
600 ~~difficult to characterize otherwise.~~

601 **GLO-Roots enables a multi-dimensional understanding of root biology**

602 Recent studies of root systems has emphasized structural attributes as important contributors
603 of root system function. Indeed, studies examining the role of genetic variants in tolerating
604 abiotic stress have demonstrated the importance of such characteristics. Roots, however, are
605 highly diverse in the biology they perform and a multi-dimensional understanding of root
606 systems, which incorporates differences in signaling, metabolism and microbial association
607 as well as structure, may provide a clearer understanding of the degree to which sub-
608 functionalization of the root system plays a role in important processes such as acclimation
609 and efficient resource acquisition.

610 We have developed tools in GLO-Roots that allow for tracking multiple aspects of soil
611 physicochemical properties and root biology simultaneously. Using GLO-Roots, we are able
612 to map in 2D coordinates soil physical properties such soil moisture together with root
613 architecture traits such as directionality, growth rates and gene expression levels. All this
614 information is aggregated in layers for each x, y coordinate. Using GLO-RIA we integrate this
615 multilayer information, leveraging our ability to simultaneously and seamlessly investigate
616 root responses to environmental stimuli such as soil moisture content. Luciferase isoforms
617 that emit light at different wavelengths allow for constitutive and regulated promoters to be
618 studied together. Introduction of luciferase reporters into microbes provides an additional
619 layer of information that provides a readout on the association between organisms and how

620 this might be affected by environmental conditions. The flexibility of the GLO-Roots system
621 may enable additional dimensionality to our understanding of root biology. Other physical
622 properties such as CO₂ or pH mapping in rhizotrons have already been enabled by using
623 planar optodes⁴¹²⁷. It may be possible to engineer LUX-based reporters in microbes that are
624 responsive to extracellular metabolites, creating microbial biosensors, and integration of such
625 tools may enable root-exudation and nutrition to be analyzed in soil. Split-Luciferase reporters
626 have been engineered that allow bi-molecular interactions to be studied. Finally, molecular
627 sensors analogous to FRET sensors, termed BRET-sensors⁴²²⁸, may allow metabolite tracking
628 dynamically through the root system. With additional innovation in the development of
629 luciferase reporters, the GLO-Roots systems will likely expand the repertoire of biological
630 processes that can be studied over an expanded range of developmental time points and
631 environmental conditions.

632 **Limited phosphorus availability promotes foraging in upper layers of soil**

633 Phosphorus availability is one of the major limitations for plant growth and an important
634 factor influencing root architecture⁴³. P is usually more abundant in the top layers of the
635 soil where it is bound to organic matter and clay minerals. Modeling studies have suggested
636 that an increase in lateral root density and shallower root systems promote phosphorus
637 uptake since phosphorus diffusibility is limited in soil and this nutrient tends to accumulate
638 in the upper tiers of the soil column where decomposition of organic matter replenishes the
639 supply of P^{10,44}.

640 Experiments using in vitro grown *Arabidopsis* seedlings have shown that the primary root
641 will senesce during low-P stress while lateral root growth is enhanced, however the total root
642 system area is often highly reduced. This change in root development would be expected to
643 reduce energy input into the root system, but provide little advantage in absorbing additional
644 phosphorus. Using GLO-Roots, we demonstrate that *Arabidopsis* does indeed have a robust
645 low-P response that we predict to enhance phosphorus uptake. While root system area is
646 not significantly reduced, root system width-depth ratio is increased, generating a shallower

647 root system. Differences between in vitro and GLO-Roots root systems may be a result of
648 the more physiologically realistic manner in which phosphorus is released to the root when
649 phosphate buffered alumina particles are used³⁵.

650 **Enhanced root growth and gravitropism may constitute an avoidance mechanism
651 used during drought**

652 It has been proposed that plants with steep root systems will be better able to tap into
653 deep water resources and thus perform better under water deprivation. For example in rice,
654 the IR64 paddy cultivar shows shallow root systems in upland fields whereas Kinandang
655 Patong, an upland cultivar, is deeper rooting⁹⁸. Plants maintain a number of regulatory
656 pathways that mediate changes in physiology during WD. Enhanced growth of root systems
657 has been well characterized in field-grown plants; however this has not been recapitulated
658 in studies of gel-grown Arabidopsis plants. Thus, it has been unclear whether Arabidopsis
659 simply responds to WD differently. Our results here show that Arabidopsis does indeed
660 maintain a classical WD response that expands the root system and directs growth downward.
661 Interestingly, under our stress regime, we did not observe a significant decrease in the relative
662 water content of shoot tissues (Figure 41-Supplement-27-figure supplement 5), suggesting
663 that the changes in root architecture were sufficient to provide access to deep water and
664 prevent dehydration. Such changes in root growth are likely regulated through systemic and
665 local signaling that involve auxin signaling but acts independently of known pathways that
666 control moisture-directed root growth.

667 **Perspectives and Conclusions**

668 Understanding plant biology requires a sophisticated understanding of how environmental
669 stimuli affect the form and function of plants as well as an understanding of how physiological
670 context informs such responses. Environmental conditions are at least as complex as the
671 plants they affect. Plant roots are exposed to a variety of environmental signals that change
672 in time and space at very different scales that are integrated at the whole plant system. It is

673 an important challenge in biology to develop methods of growing and studying plants that
674 present such stimuli in a manner that the plant is likely to encounter in nature. After all,
675 the plants we study have evolved to survive through mechanisms that have been selected,
676 over evolutionary time, in nature. ~~Use of artificial conditions must be carefully considered~~
677 ~~especially if adaptive mechanisms are the area of focus for the study.~~

678 ~~The study presented here shows conclusively that root biology in soil-like media is distinct~~
679 ~~from in vitro grown plants. These differences are not only due to media composition but~~
680 ~~likely encompass effects from other abiotic and biotic factors as well.~~ It will be interesting for
681 future studies to determine how other environmental stimuli affect root growth using GLO-
682 Roots and whether these responses differ between accessions of Arabidopsis. Identification
683 of the genetic loci responsible for phenotypic variation in adult root phenotypes may identify
684 the molecular basis for adaptive variation that exists in this species and potentially identify
685 loci that are useful for breeding efforts needed for the next green revolution.

686 Materials and methods

687 Growth system

688 **Rhizotrons and growth system fabrication.** Rhizotrons are composed of two sheets of
689 1/8" abrasion resistant polycarbonate plastic (Makrolon AR (R)) cut to size using a water
690 jet (AquaJet LLC, Salem, OR), two acrylic spacers cut using a laser (Stanford Product
691 Realization Lab), two rubber U-channels cut to strips 30 cm long ([McMaster Carr part #](#)
692 [8507K33](#)) and two sheets of black 0.030" thick polypropylene sheets ([McMaster Carr part #](#)
693 [1451T21](#)) cut with a straight-edge razor blade. Rhizotron designs were drafted in Adobe
694 Illustrator (Adobe, San José, CA). The blueprints of all the parts are provided in Supplement
695 1. The top edge of each polycarbonate sheet was painted with black 270 Stiletto nail polish
696 (Revlon, New York, NY).

697 **Boxes and holders.** Rhizotrons are held vertical during plant growth in a custom rack
698 system composed of two sheets of 1/4" black acrylic plastic cut with slots for eleven rhizotrons

699 using a laser, four 3/8" PVC rods ([McMaster Carr part # 98871a041](#)) secured with PVC
700 nuts ([McMaster Carr part # 94806a031](#)) to hold the acrylic sheets horizontal. The rack is
701 placed inside a 12" x 12" x 12" black polyethylene tank ([Plastic Mart part # R121212A](#)).

702 **Rhizotron preparation** The procedure to construct a rhizotron with soil is as follows:
703 Two pieces of polycarbonate plastic are laid flat on a table with the spacers inserted. Using
704 an electric paint gun, a fine mist of water is applied to the bare polycarbonate sheets. Then,
705 using a 2 mm sieve (US Standard Sieve Series N° 10) a fine layer of PRO-MIX(r) PGX soil
706 (Premier Tech, Canada) is applied. Excess soil is discarded by gently tapping the plastic
707 against the table in a vertical position. Water is sprayed again onto the soil, then a second
708 layer of Pro-MIX is applied as before. For P deficiency experiments soil supplemented with 1
709 ml of 100 µM P-Alumina (control) and 0-P-Alumina (P deficient) was used. To prevent the
710 soil from falling out of the bottom opening, a 3 x 6 cm piece of nylon mesh is rolled into a 1
711 cm wide tube and placed at the bottom side of the rhizotron. The spacers are removed and
712 replaced by clean spacers. The two faces of the rhizotron are carefully joined together and
713 two rubber U-channels slipped on to clamp all pieces together. Assembled rhizotrons are
714 placed into the rack inside the boxes and 500 mL of water is added to the box.

715 **Plant growth** *Arabidopsis thaliana* seeds were stratified for 2 d at 4 °C in Eppendorf tubes
716 with distilled water. Seeds were suspended in 0.1 % agar and 5 to 10 were sown using a
717 transfer pipette in the rhizotron. A transparent acrylic sheet was mounted on top of the box
718 and sealed with tape to ensure high humidity conditions that enable *Arabidopsis* germination.
719 Three days after sowing, the cover was unsealed to decrease humidity and allow the seedlings
720 to acclimate to a dryer environment. From 3 days after sowing (DAS) to the time the first
721 true leaves emerged, it was critical to ensure that the top part of the rhizotron remained
722 humid for proper germination of the plants. Between three and five DAS the rhizotrons
723 were thinned leaving only the number plants required for that experiment, typically one,
724 except for experiments examining root-root interactions. Unless otherwise stated, all the
725 experiments presented here, treatments were started 10 DAS. Plants were grown under long
726 day conditions (16 h light / 8 h dark) using 20–22 °C (day/night) and 150 µE m⁻¹ s⁻¹. Two

727 types of growth environments were used for experiments. A walk-in growth chamber with
728 fluorescent lightning and a growth cabinet with white LED lights. Relative water content
729 measurements were done as previously described^{???}

730 **qRT-PCR analysis.**

731 Seeds were surface sterilized as described before² and grown in rhizotrons, 100 cm³ pots, or
732 on two types of 1% agar (Duchefa) media containing either 1x MS nutrients (Caisson) and 1%
733 Sucrose, (termed ms media) or ¼x MS nutrients only (termed ms25 media). Both media were
734 buffered using 0.5 g/L MES and pH was adjusted to 5.7 with KOH. All plants were grown
735 together in a growth cabinet with LED lights under long day conditions (16h day/8h night).
736 Root and shoot tissue was collected separately from individual plants at the end of the day
737 (1 hour before the lights shut off) and at the end of the night (1 hour before lights came on).
738 Three biological replicates were collected for each condition. RNA was extracted using the
739 Plant RNA MiniPrepTM kit (ZYMO Research) according to manufacturer's instructions
740 with on-column DNase treatment (Qiagen). cDNA was made using the iScript Advanced
741 cDNA Synthesis for RT-qPCR kit (Bio-Rad) from 200 ng of total RNA. qRT-PCR was
742 performed using a Fluidigm BioMarkTM 96.96 Dynamic Array IFC with the EvaGreen®
743 (Bio-Rad) fluorescence probe according to the Fluidigm Advanced Development Protocol
744 number 37. For the analysis, all the reactions with no amplification (Ct =999) were either
745 removed (if the other technical duplicate amplified) or set to the maximal Ct for that assay
746 type. The two technical replicates were then averaged and dCt values calculated using
747 AT3G07480, AT4G37830, At1g13320 and At1g13440 as reference internal controls. PCA
748 plots were generated with Devium Web⁴⁵²⁹ using log dCt values. Primers used are listed in
749 file Supplement 8.

750 **Biological components**

751 **Codon optimization of luciferases.** The following luciferases that emit light at different
752 wavelengths were codon optimized for Arabidopsis (Genscript, Piscataway, NJ): LUC2: a

753 yellow improved version (Promega, Madison, WI) of the original *Photinus pyralis* (firefly)
754 LUC.

- 755 • Ppy RE8: a red variant⁴⁶³⁰ of the *P. pyralis* thermostable variant Ppy RE-TS⁴⁷³¹.
- 756 • CBG99: a green variant (Promega, Madison, WI) from yellow click beetle (*Pyrophorus*
757 *plagiophthalmus*) luciferases.
- 758 • CBR: a red variant (Promega, Madison, WI) from yellow click beetle.

759 **Non-optimized luciferases.** We also used the following non-optimized luciferases:

- 760 • nanoLUC: a blue luciferase isolated from a deep sea shrimp⁴⁸³².
- 761 • venusLUC2: a venus-LUC2 fusion reported to show higher luminescence output than
762 LUC2²³¹⁰.
- 763 • A transposon containing the bacterial luciferase-containing LUX operon was integrated
764 into the *Pseudomonas fluorescens* CH267³²²⁰ genome by conjugation with *E. coli*
765 *SM10pir* containing pUT-EM7-LUX⁴⁹³³ and used to track root microbe colonization.
766 For inoculation 9 DAS plants were inoculated with 2 mL of an overnight bacterial
767 culture resuspended in 10 mM MgSO₄ and diluted to 0.01 OD.

768 **Generation of single-reporter transgenic plants.** We generated transcriptional fu-
769 sions of all luciferases to constitutive promoters to examine the activity level and emission
770 spectrum of each isoform. The *attL1-attL2** entry clones containing plant-codon optimized
771 coding sequence of *LUC2*, *PpyRe8*, *CBG99* and *CBR* were synthesized by Genscript. A
772 DNA fragment including the *UBQ10* promoter region and first intron was amplified from
773 Col-0 genomic DNA with primers incorporating the attB1, attB4 combination sites at the
774 5' and 3' respectively. The PCR product was then introduced into pDONR™ P4-P1R
775 (Invitrogen) through a classic Gateway BP-reaction. The resulting plasmid, the *attL1-attL2*
776 entry clones with luciferase sequences, an empty *attR2-attL3** entry clone and the destination

777 vector dpGreenmCherry² were used to construct *ProUBQ10:LUC2o*, *ProUBQ10:PpyRE8o*,
778 *ProUBQ10:CBG99o* and *ProUBQ10:CBrO* through Gateway LR reactions. The destination
779 vector *dpGreenmCherry* contains a plasma membrane-localized mCherry coding sequence
780 driven by the 35S promoter and is used as a selectable marker of transformation at the
781 mature seed stage². We used Golden Gate cloning and the destination vectors that we had
782 generated before²⁴¹¹ for the following fusions: *ProUBQ10:nanoLUC2*, *ProUBQ10:venusLUC*,
783 *ProACT2:PpyRE8o*. Briefly, the different components of each construct were PCR amplified
784 with complementary BsaI or SapI cutting sites, mixed with the destination vector in a single
785 tube, digested with either BsaI or SapI, ligated with T4 DNA ligase, then transformed
786 into E. coli Top10 cells and plated on LB antibiotic plates containing X-gal as previously
787 described²⁴¹¹. Junction sites were confirmed by sequencing. We used pSE7 (Addgene
788 ID #: pGoldenGate-SE7: 47676) as the destination vector of the *ProUBQ10:nanoLUC2*,
789 *ProUBQ10:venusLUC* constructs and pMYC2 (Addgene ID #: pGoldenGate-MCY2: 47679)
790 as the destination vector for *ProACT2:PpyRE8o*. Maps of all the vectors can be found in
791 Supplement 8. *ProUBQ10:LUC2o* was transformed into Col-0, Bay and Sha accessions, the
792 *tir1-1*⁵⁰³⁴ mutant and the *miz1*⁵¹³⁵ T-DNA insertion line (SALK_126928).

793 **Brachypodium distachyon** The Arabidopsis plant-codon optimized Luciferase gene,
794 *LUC2o*, was inserted into the monocot vector pANIC10 via Gateway cloning²⁹¹⁵. *Brachy-*
795 *podium distachyon* plants were transformed using the method of Vogel and Hill⁵²³⁶.

796 **Tomato** The transcriptional fusion *ProeDR5:LUC2* was generated by cloning the
797 *ProeDR5:LUC2* DNA fragment into the pBIB expression vector via restriction sites SalI
798 and Acc65I. The eDR5 promoter is an enhanced version of DR5 containing 13 repeats
799 of the 11-nucleotide core DR5 element⁵³³⁷ and the pBIB expression vector contains an
800 NPTII resistance gene under the control of the NOS promoter for use as a selectable
801 marker during transformation. ~~This construct was transformed into the XYZ cultivar of~~
802 ~~tomato~~ All tomato transformations were performed by the Ralph M. Parsons Foundation
803 Plant Transformation Facility (University of California, Davis).

804 **Generation of dual-reporter plants.**

805 To generate dual-reporter plants expressing luciferase isoforms that emit light with di-
806 vergent emission spectra we used *ProACT2:PpyRE8o* as the root structural marker and
807 ZAT12:LUC³⁴¹⁹ and DR5:LUC+³³¹⁸ lines that were transformed with the *ProACT2:PpyRE8o*
808 construct. All constructs were transformed using a modified floral dip method as described
809 in².

810 *Tomato*

811 The *Pro35S:PpyRE8o* transcriptional fusion was generated by putting the plant-codon
812 optimized coding sequence described above into the pMDC32 expression vector through a
813 Gateway LR reaction. The pMDC32 vector contains a hygromycin resistance gene under
814 the control of the 35S promoter for use as a selectable marker during transformation. This
815 construct was transformed into the transgenic *ProeDR5:LUC2* tomato line. ~~All tomato~~
816 ~~transformations were performed by the Ralph M. Parsons Foundation Plant Transformation~~
817 ~~Facility (University of California, Davis).~~

818 **In vivo emission spectra of plants constitutively expressing luciferase isoforms.**

819 To generate *in vivo* emission spectra of all constitutively expressed luciferases, seeds were
820 sterilized and sown on MS plates as described before². After 8 days, seedlings were treated
821 with a 100 µM luciferin solution, incubated at room temperature for 3 hours and imaged
822 using an IVIS Spectrum imaging system (Perkin Elmer, bla, bla) using 20 nm band-pass
823 emission filters at the following wavelengths (in nm: 490-510, 510-530, 530-550, 550-570,
824 570-590, 590-610, 610-630, 630-650, 650-670, 670-690, 690-710). Raw images were analyzed
825 using Fiji and *in vivo* emission spectra were constructed. The full emission spectra of LUX
826 and nanoLUC could not be constructed since the maximum of these two luciferases is below
827 the lower band pass filter that were available.

828 **Imaging system**

829 We designed a custom imaging system (GLO1, Growth and Luminescence Observatory 1)
830 optimized for imaging dual-reporter luciferase expression in our custom rhizotrons. The
831 design was a joint effort with Bioimaging Solutions (San Diego, CA) who also built the
832 system and wrote the acquisition software that drives all the mechanical parts of the system.
833 The system is composed by two 2048 x 2048 PIXIS-XB cameras (Princeton Instruments,
834 Trenton, NJ) mounted on top of each other to capture two fields of view encompassing
835 approximately two 15 x 15 cm areas corresponding to the top or bottom of the rhizotron.
836 The cameras are fitted with a Carl-Zeiss macro lens. A filter wheel with space for four,
837 76.2 mm filters is positioned in front of the cameras and controlled by a stepper motor
838 allowing for automated changing of the filter wheel position. We used two -542/50 and
839 450/70- custom cut Brightline(R) band-pass filters (Semrock, Rochester, NY). In single color
840 imaging mode, the filter wheel is operated without filters. Positioned in front of the filter
841 wheel is a removable rhizotron holder mounted on a stepper motor. This stepper motor is
842 also controlled by the GLO-1 software allowing automatic acquisition of images from both
843 sides of the rhizotron sequentially. The whole imaging system is enclosed in a light-tight
844 black box with a door that allows loading and un-loading of rhizotrons.

845 **Plant Imaging**

846 Around 50 mL of 300 µM D-luciferin (Biosynth, Itasca, IL) was added to soil at the top of
847 the rhizotron. In general 5 min exposures were taken per rhizotron, per side, per channel.
848 For daily imaging experiments, plants were imaged at dawn (+/- 1 hr) to reduce possible
849 effects on diurnal rhythms of keeping plants in the dark during imaging. Shoot images were
850 taken using a Nikon D3100 camera.

851 **Image Preparation**

852 Four individual images are collected: top front, bottom front, top back and bottom back~~and~~.
853 Using an automated ImageJ macro, a composite image is generated as follows: 1) To correct
854 for differences in background values between the two cameras the mean background value of
855 each image is subtracted from 200; 2) images are rotated and translated to control for small
856 misalignments between the two cameras; 3) the top and bottom images of each side are
857 merged; 4) the back image is flipped horizontally; 5) the front and back images are combined
858 using the maximum values. When dual color images are acquired this operation is repeated
859 for each channel. The final images produced are 16-bit depth and 4096 x 2048 pixels. The
860 scale of the images is 138.6 pixels per cm. Considering that an Arabidopsis roots is 100 µm
861 this results in 1.39 pixels across an Arabidopsis root.

862 **GLO-RIA imageJ plug-in**

863 ~~The GLO-RIA plugin is divided in two parts:~~

864 ~~The first part (RootSystem) performs four different types of analysis: i) local analysis~~
865 ~~detects all root particles in the image and computes their position, length and direction;~~
866 ~~ii) the global analysis performs a root system level analysis and computes the total visible~~
867 ~~surface, convex hull, width and depth; iii) the shape analysis uses a combination of~~
868 ~~existing tools to extract relevant root architecture features. Directionality is acquired using~~
869 ~~the directionality plugin from ImageJ. After the number of direction bins (we usually use~~
870 ~~bins of 2 °) is defined by the user, a 5x5 sobel operator is used to derive the local gradient~~
871 ~~orientation. This orientation is then used to build a distribution of directions by assigning~~
872 ~~the square of the orientation into the appropriate bin. Instead of representing the total~~
873 ~~counts at each orientation a relative value is calculated by dividing the individual values at~~
874 ~~each bin by the total sum of the histogram (and multiplying by 100). Similar algorithms~~
875 ~~have been used to quantify dynamic changes in the plant cytoskeleton³⁸.~~

876 ~~The Elliptic Fourier Descriptors to perform a shape analysis on are aquired using the~~
877 ~~Fourier Shape Analysis plugin on convex hull shape of the root systemconvex hull iv) the~~

878 directionality analysis computes the mean direction of root particles in a. Elliptic Fourier
879 Descriptors have been used in numerous studies to analyse variations in shapes, notably in
880 leaves (e.g.???) The shape analysis is inspired by RootScape???. Due to the absence of fixed,
881 recognisable structures in root system (either on the full image or by user-defined sections
882 of the image). These four analysis are fully automated by default, but can be manually
883 adjusted if needed.

884 The second part of GLO-RIA (RootReporter) was specifically designed for the analysis of
885 dual reporter images (gene reporter and a root structural reporter) that are required for
886 the position of true landmarks), pseudo-landmarks are automatically extracted from the
887 root systems. Shortly, the plugin works as follow: i) detection of the gene reporters and
888 the structure reporters in their respective images; ii) if needed, a manual correction can
889 be performed to correct the automated detection; iii) gene reporters are linked with the
890 structure reporters, based on their proximity; iv) gene reporter intensity (either absolute or
891 normalized using the structural reporter) is computed; v) all data are exported and saved to
892 an RSML datafile⁵⁴. Gene and structure reporters can be followed across different time and
893 space points. image is divided vertically at equidistant positions (with the number defined by
894 the user) and for each of the image stripes, the minimum and maximum x coordinates are
895 computed. The shape analysis is therefore able to discriminate root system with different
896 vertical root distributions or global root system orientation (e.g. chemotropism). The code
897 source for the plugin, manual and sample images can be found in the github repository of
898 the project.

899 Statistical analysis was performed in R⁵⁵³⁹. The tidyR⁵⁶⁴⁰, dplyr⁵⁶⁴⁰, gridExtra⁵⁷⁴¹, shapes⁴²,
900 geomorph⁴³ and ggplot2⁵⁸⁴⁴ packages were used for data preparation, analysis and plotting.
901 Final figure preparation was done in Inkscape.

902 Data availability

903 All the scripts and original^{original} data used to analyze and produce the images can be
904 accessed in the Github repository of the project: github.com/rr-lab/glo_roots. Raw files of

905 all the images used in the paper ~~is~~are availabale in [Dryad](#).

906 **Acknowledgements**

907 Work in the lab of JRD was funded by the Carnegie Institution for Science Endowment and
908 grants from the National Science Foundation (MCB-115795) and Department of Energy,
909 Biological and Environmental Research program (DE-SC0008769). RRA was supported by a
910 Carnegie Postdoc Fellowship and currently by Conacyt Ciencia Básica Joven Investigador
911 grant number (CB-2014-01-238101). GL was supported by the Belgian Fonds de la Recherche
912 Scientifique. JM was funded by the National Science Foundation (IOS-0820854). CH is
913 funded by MGH Toteston & Fund for Medical Discovery Fellowship grant 2014A051303
914 and NIH R37 grant GM48707 and NSF grant MCB-0519898 awarded to Frederick Ausubel,
915 and previously by the Gordon and Betty Moore Foundation through Grant GBMF 2550.01
916 from the Life Sciences Research Foundation. JV was funded by the Office of Biological and
917 Environmental Research, Office of Science, US Department of Energy, interagency agreements
918 DE-SC0001526 and DE-AI02-07ER64452. We thank Robert Mittler and Philip Benfey for
919 providing seeds of ZAT12:LUC and DR5:LUC+ respectively. We also thank Neil Robbins
920 for critical review of the manuscript an suggestions during the development of the project.
921 We greatly appreciate Tim Doyle´s advice and help with ~~mul~~luciferase imaging.

922 **Competing interests**

923 We do not have any competing interests that we are aware of.

924 **Tables**

925 **Table 1:** Luciferases used in this study.

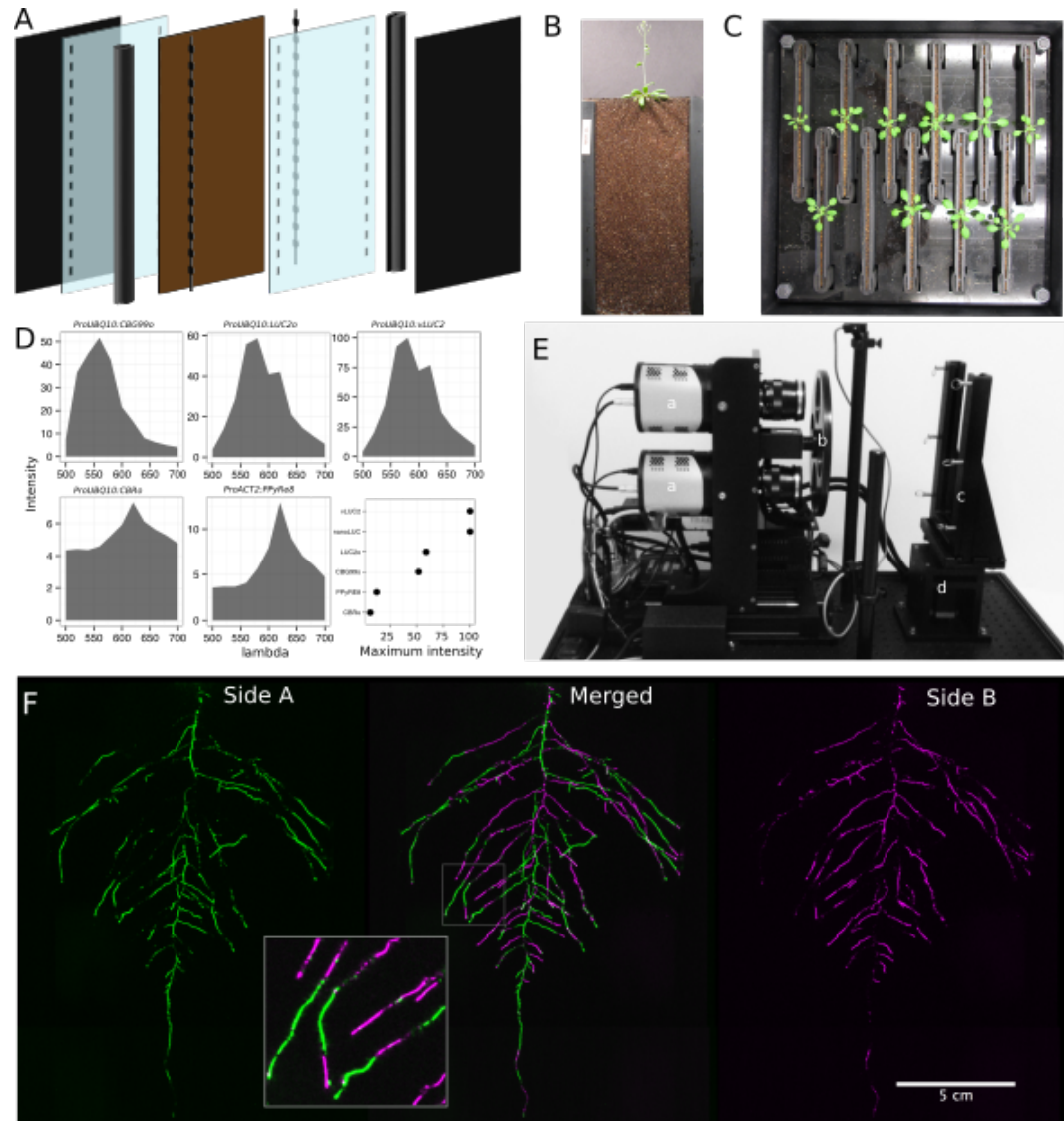
Luciferase	Origin	maximum wavelength	Substrate
Ppy RE8	firefly	618	D-luciferin

Luciferase	Origin	maximum wavelength	Substrate
CBGRed	click beetle	615	D-luciferin
venus-LUC2	FP + firefly	580	D-luciferin
LUC(+)	firefly	578	D-luciferin
CBG99	click beetle	537	D-luciferin
lux operon	A. fischeri	490	biosynthesis pathway encoded within operon
nanoLUC	Deep sea shrimp	470	firimazine

926 **Table 2:** list of root system features extracted using GLO-RIA.

variable	unit
projected area	cm ²
number of visible roots	~
depth	cm
width	cm
convex hull area	cm ²
width	cm
feret	cm
feret angle	°
circularity	~
roundness	~
solidity	~
center of mass	cm
Directionality	°
Euclidean Fourier Descriptors	~
Pseudo landmarks	~

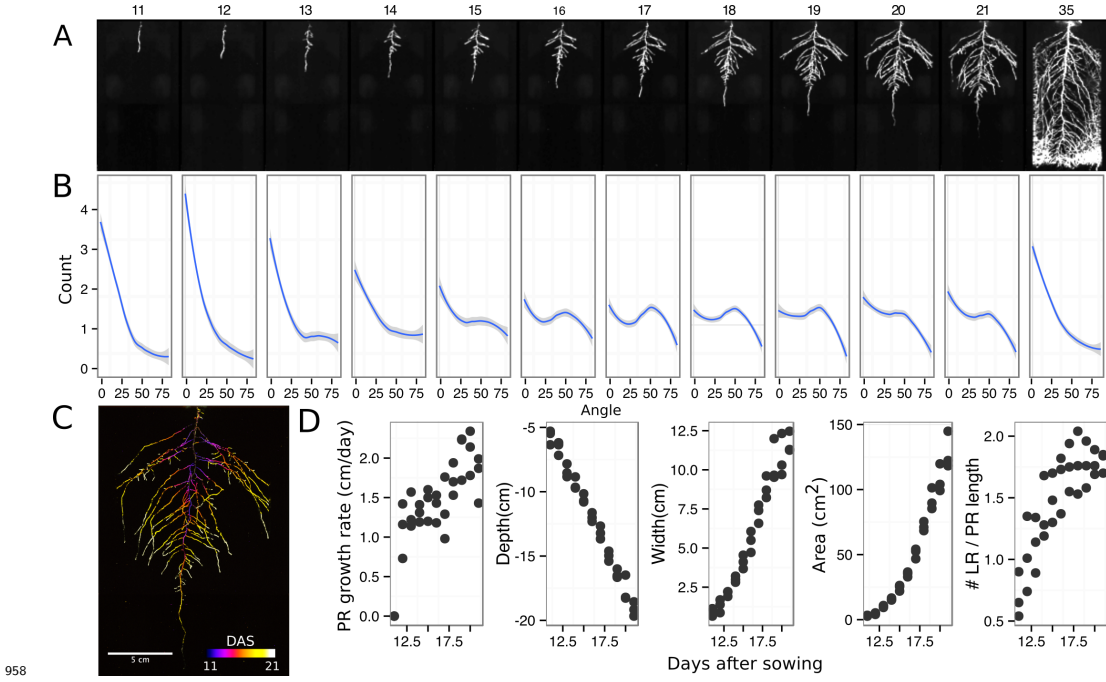
927 **Figures**



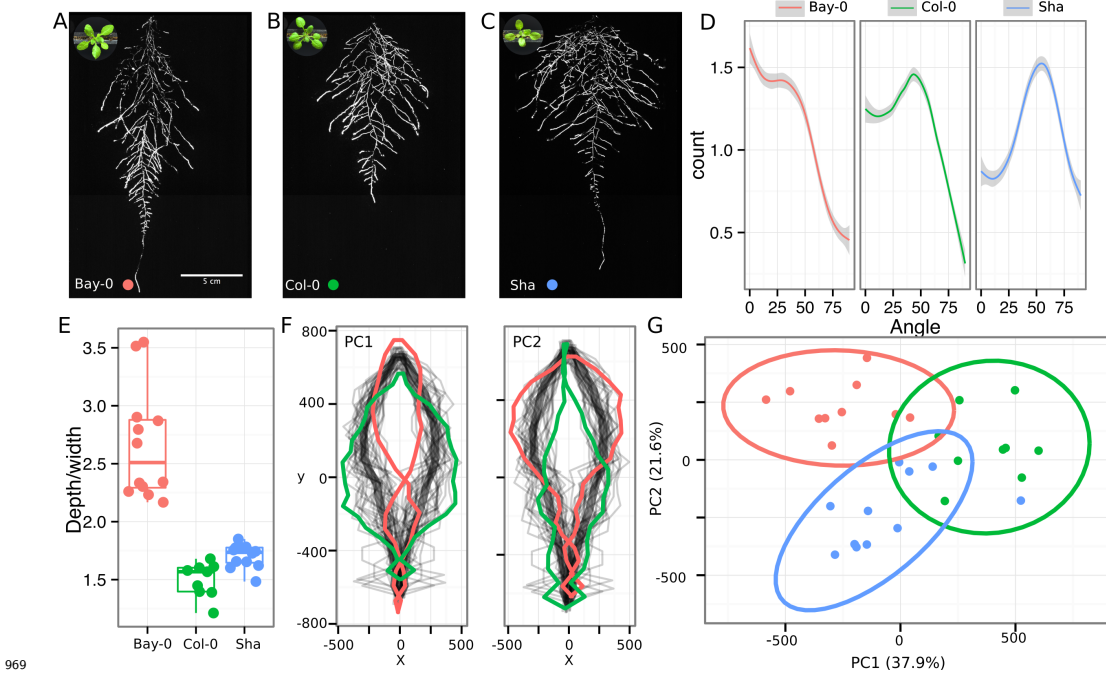
929 **Figure 1.** A) 3D representation of the different components of the rhizotron: plastic
 930 covers, polycarbonate sheets, spacers and rubber U-channels. Blueprints are provided in
 931 Supplementary material 1. In brown, soil layer. B) Thirty five days old plant in rhizotron
 932 with black covers removed. C) Top view of holding box with eleven rhizotrons. D) Principal
 933 Components Analysis (PCA) score plot of a set of 77 genes analyzed by qPCR from root
 934 samples of plants grown in MS plates, pots, and rhizotrons. After 15 DAS three plants

935 were collected at the end of the day (D) and three were collected at the end of the night
936 (N). (ms = plant grown in full ms; ms25 = plants grown in 25% of full ms) E) Heat map of
937 genes that were significantly different between rhizotrons and media in either day or night
938 or both. We used p-value < 0.00065 threshold based on Bonferroni adjustment for multiple
939 testing. F) Lateral root number and G) primary root length of 18 DAS plants grown in
940 30-cm tall cylinders, pots and rhizotrons, all with a volume of 100 cm³ (n = 6-12 plants).
941 H) Leaf area and I) primary root length of plants of the same age (15 DAS) as the ones
942 used for the qPCR experiment (n = 6-7). ANOVA analysis with p < 0.01 was used to test
943 significant differences between the different parameters.

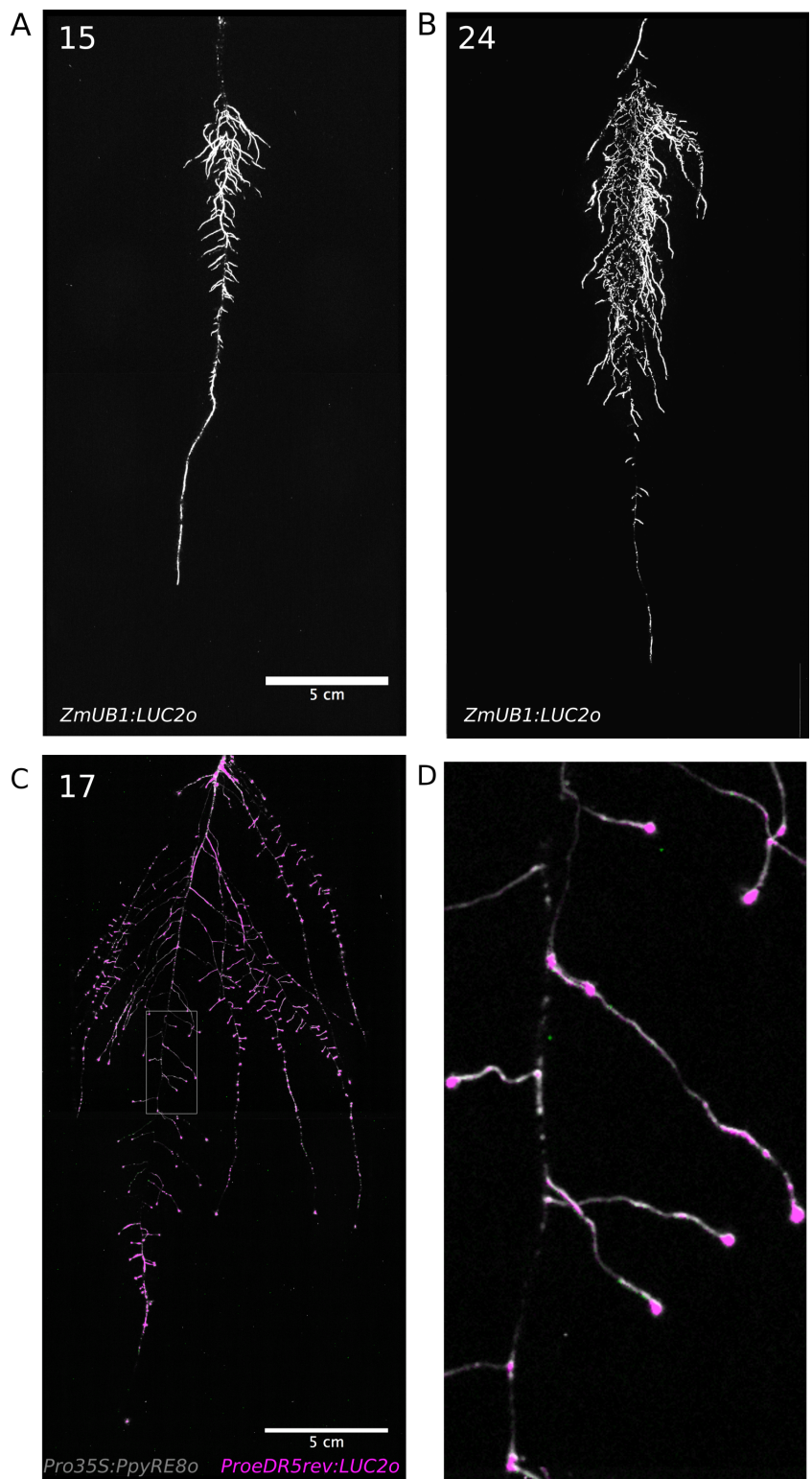
944 **Figure 2:** A) In vivo emission spectra of different luciferases used in this study. Transgenic
945 homozygous lines expressing the indicated transgenes were grown on agar media for 8 days.
946 Luciferin (300 µM) was sprayed on the seedlings and plates were kept in the dark and then
947 imaged for 2 s at wavelengths ranging from 500 to 700 nm. Five intensity values were taken
948 from different parts of the roots of different seedlings and averaged. Relative maximum
949 intensity values are indicated in the lower right graph. BE) GLO 1 imaging system. The
950 system is composed by two back illuminated CCD cameras (a) cooled down to -55 °C. A
951 filter wheel (b) allows for spectral separation of the different luciferases. On the right, a
952 rhizotron holder (c) is used to position the rhizotrons in front of the cameras. A stepper
953 motor (d) rotates the rhizotron 180° to image both sides. CF) A 21 DAS plant expressing
954 *ProUBQ10:LUC2o* was imaged on each of two sides of the rhizotron; luminescence signal is
955 colorized in green or magenta to indicate side. In the middle of the panel, a combined image
956 of the two sides is shown. The inset shows a magnified part of the root system. FW: fresh
957 weight, PR: Primary root.



958 **Figure 32.** A) Typical daily time-lapse image series from 11 to 21 DAS of a
959 *ProUBQ10:LUC2o* Col-0 plant. B) Color-coded projection of root growth using the images
960 in panel A. C) Directionality of the root system of plants in panel A calculated using the
961 directionality plugin implemented in GLO-RIA. C) Color coded projection of root growth
962 using the images in panel A. D) Primary root growth rate, depth, width, root system area
963 are automatically calculated from the convex hull, which is semi-automatically determined
964 with GLO-RIA. Lateral root number and number of lateral roots divided by the primary
965 root length were quantified manually. A Local Polynomial Regression Fitting with 95%
966 confidence interval (grey) was used to represent the directionality distribution curve. (0° is
967 the direction of the gravity vector).

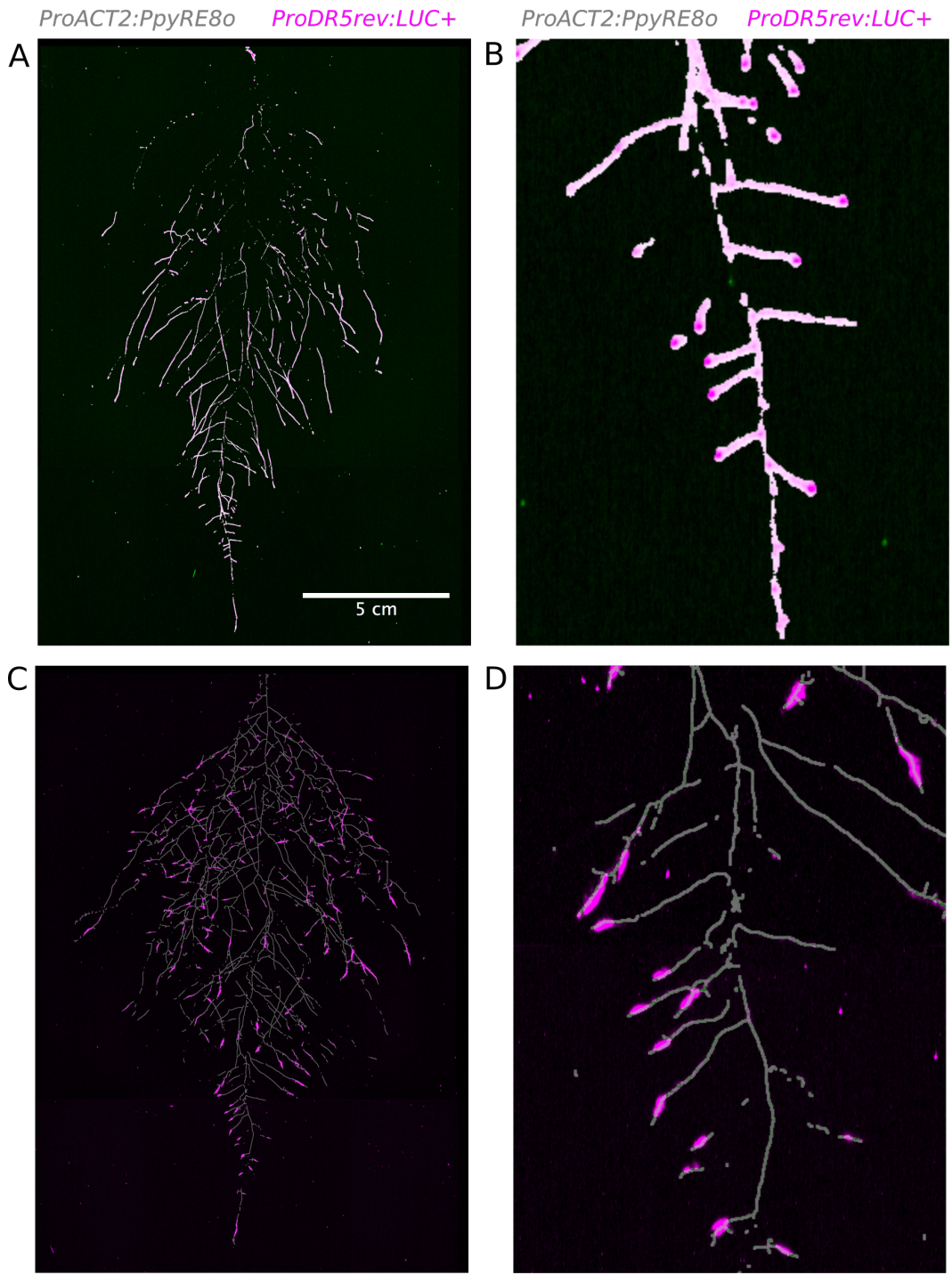


969 **Figure 43** Representative root and shoot images of A) Bay-0, B) Col-0 and C) Sha
 970 accessions 22 DAS transformed with *ProUBQ10:LUC2o*. D) Directionality of the root
 971 systems, E) ~~root area~~, F) ~~depth/width ratio~~ G) ~~vertical center of mass of Bay-0, Col-0 and~~
 972 ~~Sha accessions.~~ ANOVA analysis with $p < 0.01$ was used to test significant differences
 973 between the different parameters ($n = \text{ }$). F) Elliptic Fourier Descriptors of shape variation
 974 in root system architecture. Eigenvalues derived from the analysis of 9-12 plants per
 975 accession is shown. The first two Principal Components explaining 38% (PC1) and 22%
 976 (PC2) of the shape variation are plotted. PC1 captures homogeneity of root system width
 977 along the vertical axis with and PC2 a combination of depth and width in top parts of the
 978 root system. Red and green lines indicate $-3SD$ and $+3SD$, respectively G) PCA separation
 979 of the different ecotypes using the PC described in F. A Local Polynomial Regression Fitting
 980 with 95% confidence interval (grey) was used to represent the directionality distribution
 981 curve. (0° is the direction of the gravity vector). Wilcoxon test analysis with $p < 0.01$ was
 982 used to test significant differences between the different accession ($n = 9-12$ plants).



984

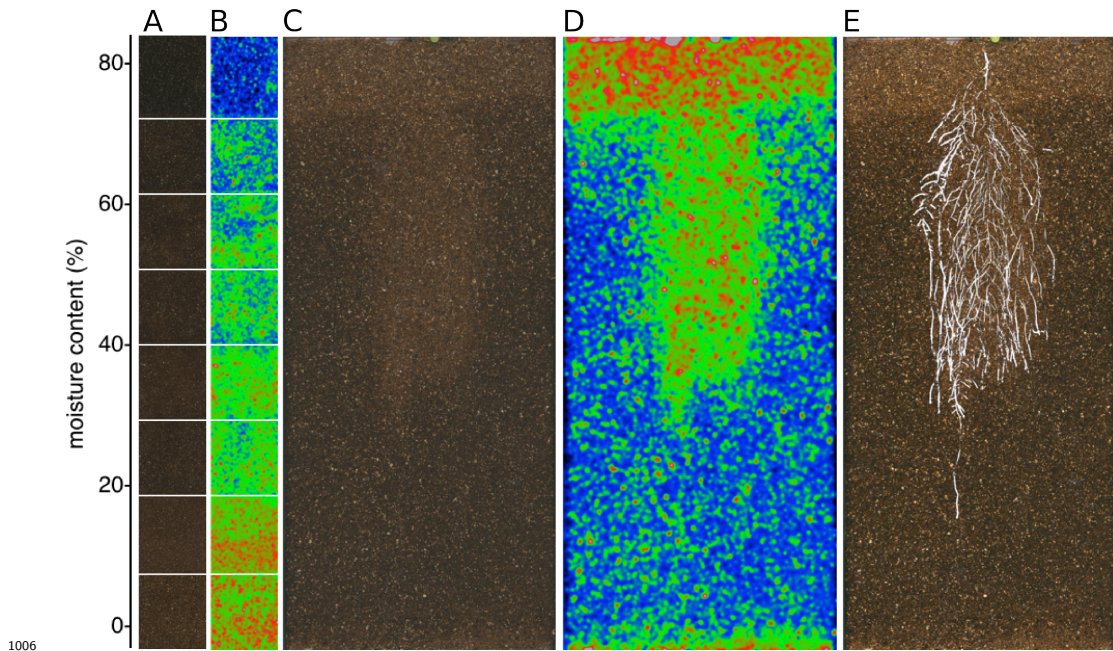
985 **Figure 54:** Roots of *Brachypodium distachyon* transformed with *ProZmUB1:LUC2o*
986 and imaged at 15 (A) and 24 (B) DAS grown in control conditions. **B)** Depth of the
987 primary root of *Brachypodium* plants grown in rhizotrons or on gel-based media (n=8-11).
988 **C)** 14 **C)** 17 DAS tomato plant transformed with *ProeDR5rev:LUC2o* (magenta) and
989 *Pro35S:PPyRE8o* (grey) D) Zoomed inset of root in panel D showing increased expression of
990 **ProeDR5rev:LUC2o** *ProeDR5rev:LUC2o* reporter in early-stage lateral roots.



992 **Figure 65:** A) Triple color picture showing a 22 DAS *ProUBQ10:LUC2o* plant (magenta)
993 grown in the same rhizotron with *ProACT2:PpyRE8o* plants (grey). Plants were inoculated

994 with *Pseudomonas fluorescens* CH267 (green) Magnified portion of root systems colonized
 995 by *Pseudomonas fluorescens* showing *P. fluorescences* (B) only or all three reporters
 996 together (C).

997 **Figure 7:** Images of whole root systems (A, C) or magnified portion of roots (B, D) at 22
 998 DAS expressing *ProDR5rev:LUC+* (magenta, A, B) or *ProZAT12:LUC* signal (magenta, C,
 999 D) with skeletonized representation of root roots generated using the *ProACT2:PpyRE80*
 1000 reporter expression (in grey) E) Time series showing root growth and *ProZAT12:LUC*
 1001 expression after salt addition to the right side of the root system. F) Correlation of root
 1002 growth and *ProZAT12:LUC* expression intensity. E) Visualization of the results obtained
 1003 by analyzing the ZAT12:LUC image with the GLO-RIA Root Reporter module. Blue circles
 1004 are proportional in size to the ZAT12:LUC intensity value. Hovering over the points will
 1005 reveal numerical values for the ZAT12:LUC intensity

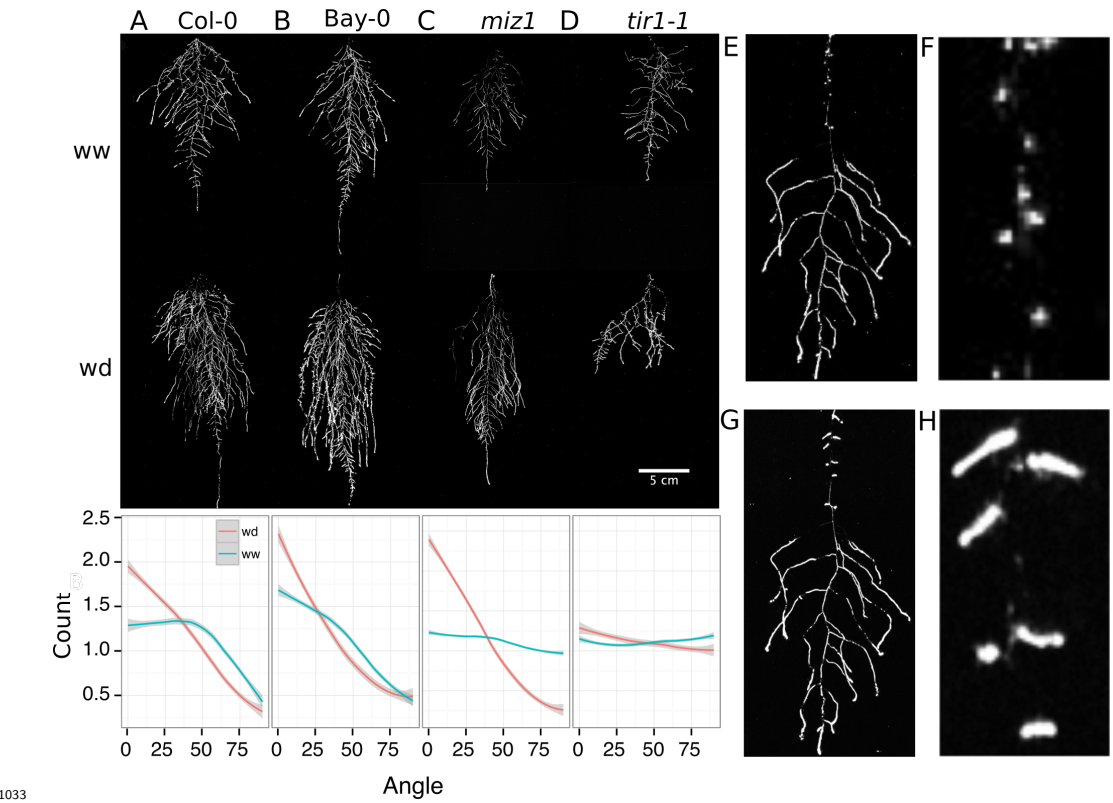


1006
 1007 **Figure 8:** Shoot and root systems of *ProUBQ10:LUC2o* Col-0 plants growing in soil
 1008 supplemented with 1ml of 100 µM P-Alumina (left) and 0-P-Alumina (right) 22 (A) or 27 (B)
 1009 DAS. C) Root depth/width ratio of 22 (top) and 27 (bottom) DAS plants. D) Scatter-plot
 1010 showing relationship between root and shoot system area at 22 (top) and 27 (bottom) DAS.

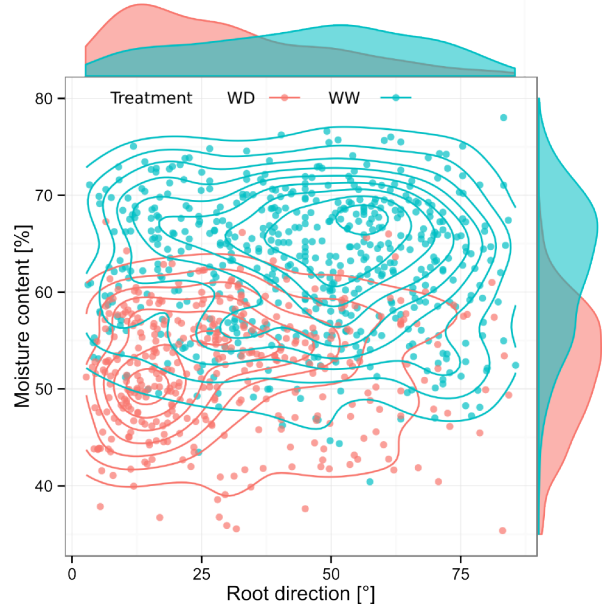
1011 E) Root directionality distribution in plants 22 (top) and 27 (bottom) DAS. Anova analysis
1012 at $p < 0.01$ was used to compare depth/width ratios in P treatments. Kolmogorov-Smirnov
1013 test at $p < 0.001$ was used to compare directionality distributions between the different
1014 treatments. A Local Polynomial Regression Fitting with 95% confidence interval (grey)
1015 was used to represent the directionality distribution curve. (0° is the direction of the gravity
1016 vector).

1017 **Figure 9.** A) Col-0 root systems shielded (top) or light exposed (bottom). After 9 DAS
1018 the top third of the rhizotron was exposed to light (indicated on the side with a light grey
1019 bar) and plants were imaged at 20 DAS. B) Directionality analysis of root systems shielded
1020 (red) or exposed (green) to light for Col-0 (top panel) or phot1/2 double mutant (bottom
1021 panel). Between 4 and 6 plants were analyzed per treatment. ANOVA analysis at $p < 0.01$
1022 was used to compare depth/width ratios in P treatments. Kolmogorov-Smirnov test at p
1023 < 0.001 was used to compare directionality distributions between the different treatments.
1024 A Local Polynomial Regression Fitting with 95% confidence interval (grey) was used to
1025 represent the directionality distribution curve. (0° is the direction of the gravity vector).

1026 **Figure 106:** Soil moisture mapping in rhizotrons. A) Composite image strip made from
1027 rhizotrons prepared with different soil moisture levels. B) Differences in grey-scale intensity
1028 values were enhanced using a 16-color Look Up Table (LUT). Brightfield image of soil in
1029 rhizotron (C) and converted using 16-color LUT to enhance visualization of distribution of
1030 moisture (D) . E) Root system of a Bay-0 22 DAS and subjected to water deprivation since
1031 13 DAS. Root system visualized using luminescence and overlaid on brightfield image of soil
1032 in (C).



1033 **Figure 117:** A-D) Root systems 22 DAS and exposed to water deficit 13 DAS onwards.
 1034 Sample images of well watered (left panels) and water deficit (right panels) root systems
 1035 started 13 DAS and directionality (line graphs to left of images) for (A) Col-0 (B) Bay-0
 1036 (C) *miz1* mutant and (D) *tir1-1*. E) Root system of a 22 DAS plant exposed to water
 1037 deprivation from 9 DAS onwards with magnified view of lateral root primordia (F). G) The
 1038 same root as in (E) 24 hours after rewatering and magnified view of lateral root primordia
 1039 (H). Kolmogorov-Smirnov test at $p < 0.001$ was used to compare directionality distributions
 1040 between the different treatments and genotypes. A Local Polynomial Regression Fitting
 1041 with 95% confidence interval (grey) was used to represent the directionality distribution
 1042 curve. (0° is the direction of the gravity vector).



1044 **Figure 128:** Relationship between local soil moisture content and root growth direction.
 1045
 1046 Data quantified from the time lapse shown in [Video 3](#). Density plots shown at periphery of
 1047 graph for root direction (x-axis) and soil moisture (y-axis). (0° is the direction of the gravity
 1048 vector).

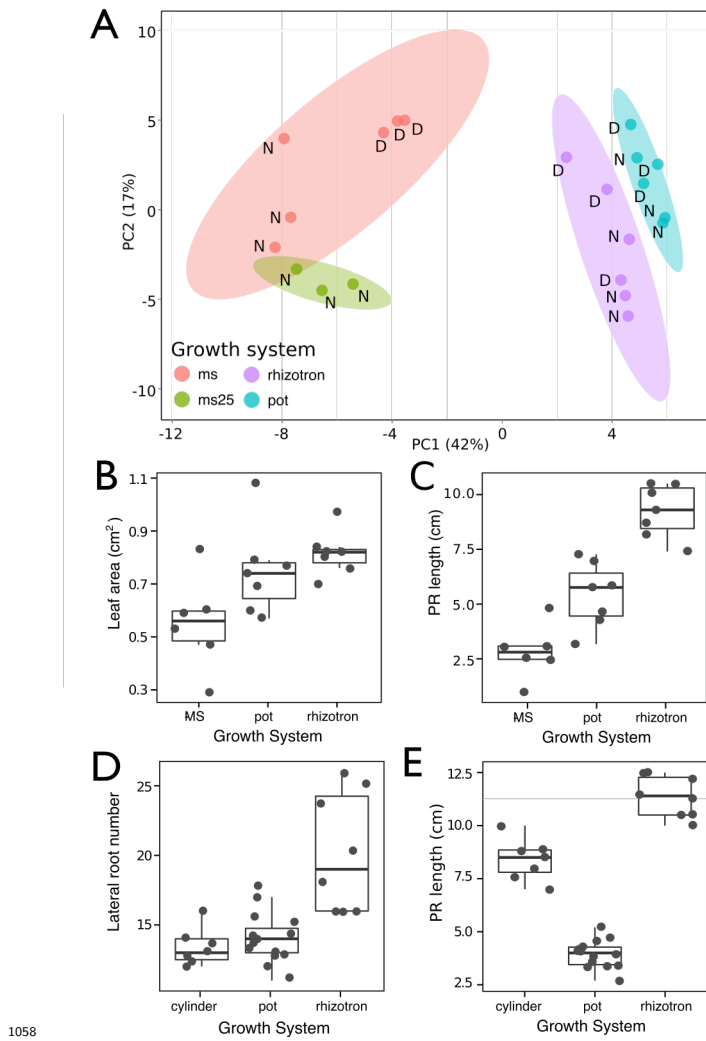
1049 Videos

1050 **Video 1** Time lapse from 11 to 21 DAS of a Col-0 plant expressing *ProUBQ10:LUC2o*
 1051 grown in control conditions

1052 **Video 2** 24 h time lapse a Col-0 plant expressing *ProACT2:PpyRE8* (gray) and *ZAT12:LUC*
 1053 (magenta) after addition of a 1 M solution of NaCl on the right side of the plant.

1054 **Video 3** Time lapse from 16 to 24 DAS of Col-0 plants expressing *ProUBQ10:LUC2o*
 1055 growing in water deficient conditions (left) and control (right). Plants were sown under
 1056 control conditions and water deficit treatment started 11 DAS.

1057 **Supplementary Material**



1058

1059 **Figure 1-figure supplement 1** **Supplement 1** PCA plot of A) Principal Components
 1060 Analysis (PCA) score plot of a set of 77 genes analyzed by qPCR from root samples of
 1061 plants grown in MS plates, pots, and rhizotrons. After 15 DAS three plants were collected
 1062 at the end of the day (D) and three were collected at the end of the night (N). (ms = plant
 1063 grown in full ms, ms25 = plants grown in 25% of full ms) B) Lateral root number and G)
 1064 primary root length of 18 DAS plants grown in 30 cm tall cylinders, pots and rhizotrons,
 1065 all with a volume of 100 cm^3 (n = 6-12 plants). D) Leaf area and E) primary root length
 1066 of plants of the same age (15 DAS) as the ones used for the qPCR experiment (n= 6-7).

1067 ANOVA analysis with $p < 0.01$ was used to test significant differences between the different
1068 parameters.

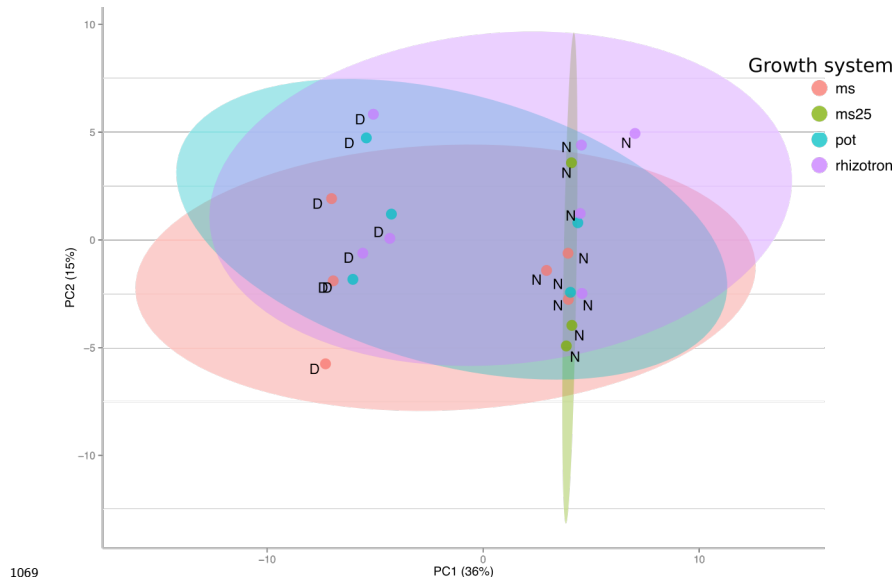
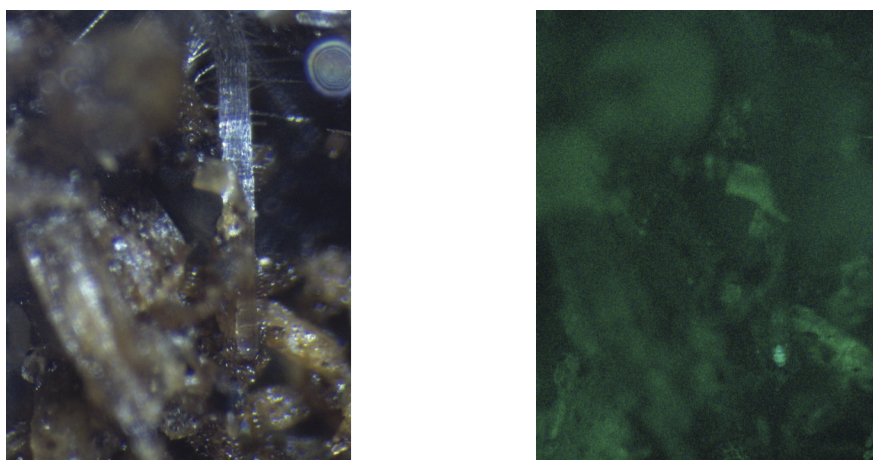


Figure 1-figure supplement 2 PCA plot of shoots of the same samples used in Figure 1.

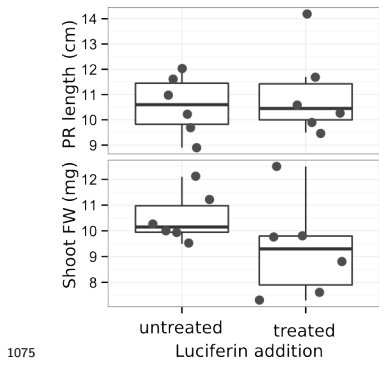
¹⁰⁷¹ See Figure 1 for more details regarding experimental conditions used.



Brightfield

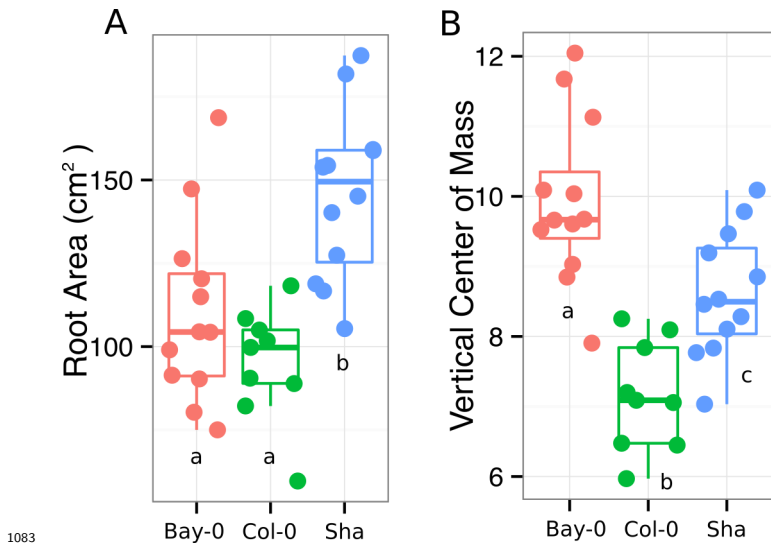
GFP

1073 **Figure 2-Supplement 11-figure supplement 3** Image of a *Arabidopsis* root in soil
1074 under white light (brightfield) and GFP excitation light.

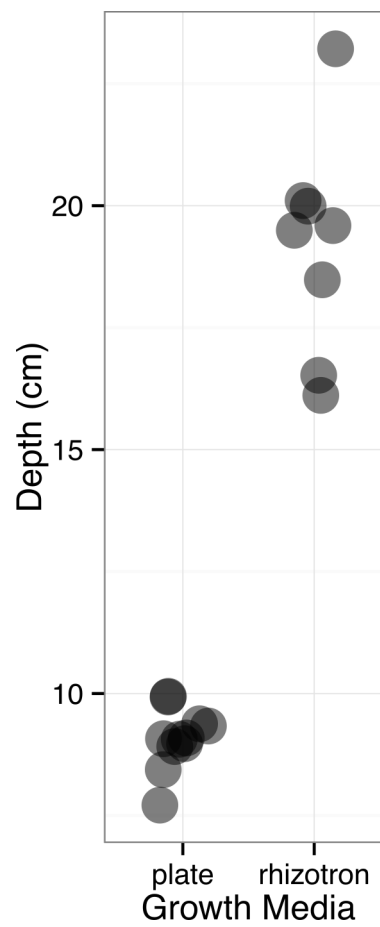


1075 **Figure 1-figure supplement 4** Effect of luciferin addition on the primary root length and
1076 shoot size of 14 DAS seedlings that were either continuously exposed to 300 μ M luciferin
1077 from 9 DAS after sowing or not.
1078

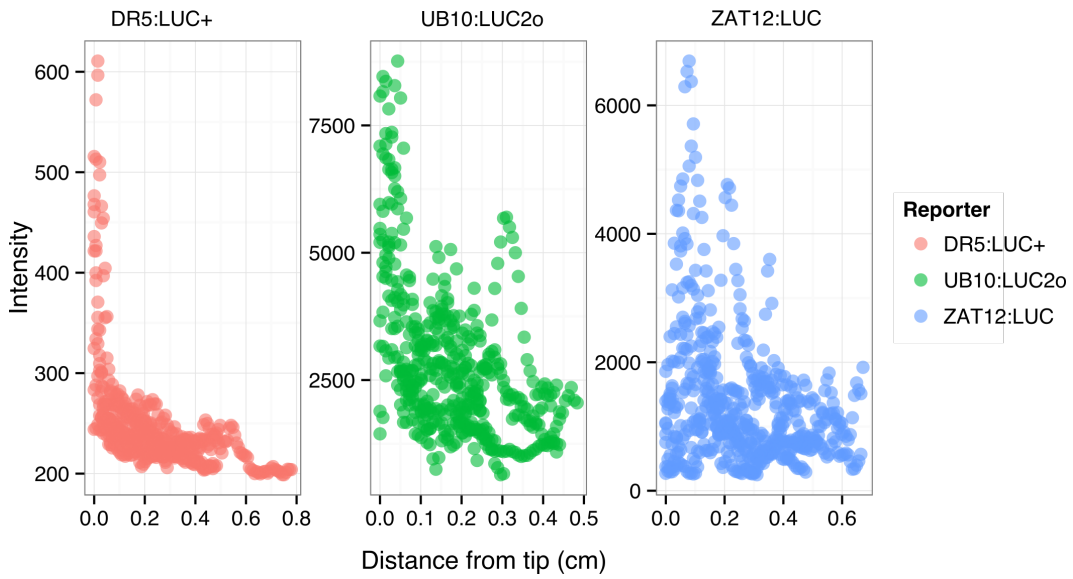
1079 **Figure 1-figure supplement_data_1:** Two way ANOVA P-values comparing plants
1080 grown in MS media vs plants grown in soil (pots or rhizotrons) and plants collected at day
1081 or night. We used p-value < 0.00065 threshold based on Bonferroni adjustment for multiple
1082 testing.



1083 **Figure 6-Supplement-3-figure supplement 1** A) root area, B) vertical center of mass
1084 of Bay-0, Col-0 and Sha accessions.
1085

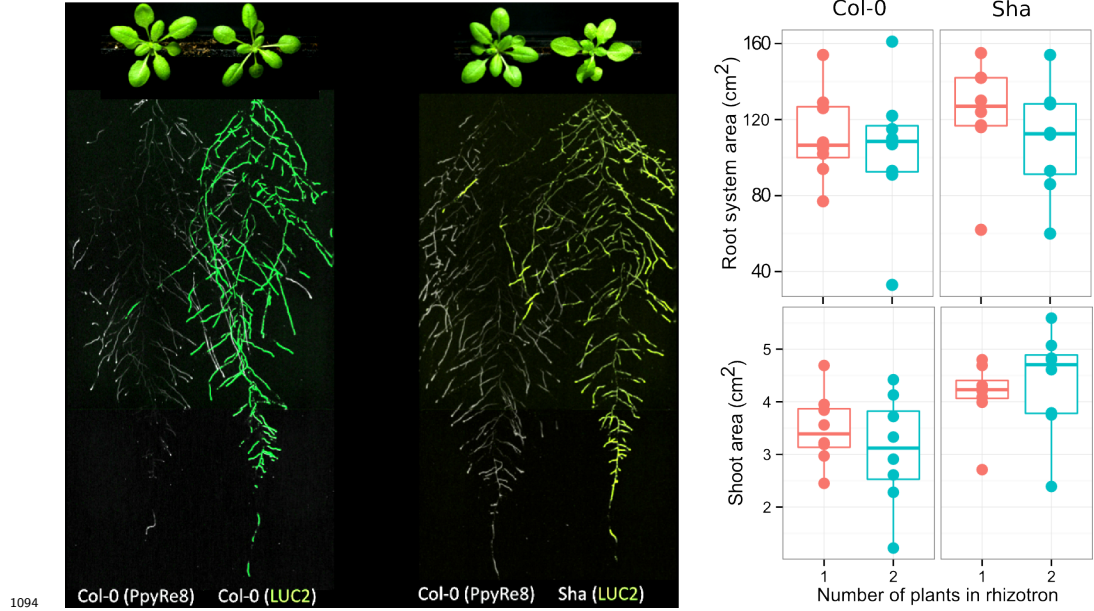


1086
1087 **Figure 4-figure supplement 1** Depth of the primary root of *Brachypodium* plants grown
1088 in rhizotrons or on gel-based media (n=8-11).



1089

1090 **Figure 5-figure supplement 1** Dual color images of 22 DAS plants growing in the
 1091 same rhizotron and expressing different luciferases. A) Two Col-0 plants expressing
 1092 *ProUBQ10:LUC2o* and *ProACT2:PPyRE8o* B) Col-0 plant expressing *ProACT2:PPyRE8o*
 1093 and Sha plant expressing *ProUBQ10:LUC2o*.



1094 **Figure 9-Supplement 15-figure supplement 2** Plots showing output of directionality
 1095 analysis performed at different depths (0-5; A) Triple color picture showing a 22 DAS
 1096

1097 *ProUBQ10:LUC2o* plant (magenta) grown in the same rhizotron with *ProACT2:PpyRE8o*
1098 plants (grey). Plants were inoculated with *Pseudomonas fluorescens* CH267 (green).
1099 Magnified portion of root systems colonized by *Pseudomonas fluorescens* showing *P.*
1100 *fluorescences* (B) only or all three reporters together (C).

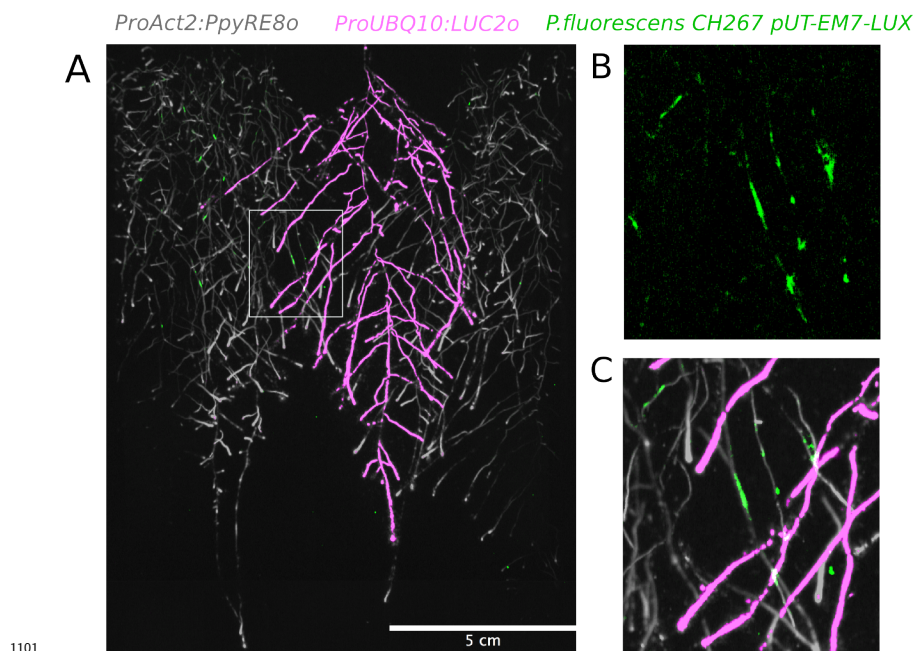


Figure 5-figure

1102 **supplement 3:** DR5:LUC+, 5–10, 10–15 cm) in rhizotrons exposed to light or kept in the
1103 dark. (0° is the direction of the gravity vector). UBQ10:LUC2o and ZAT12:LUC intensity
1104 values along the root tip. Data was manually obtained by obtaining the intensity profile of
1105 the first 0.3–0.8 cm from the root tip of individual lateral roots. Ten lateral roots for each
1106 reporter were measured.

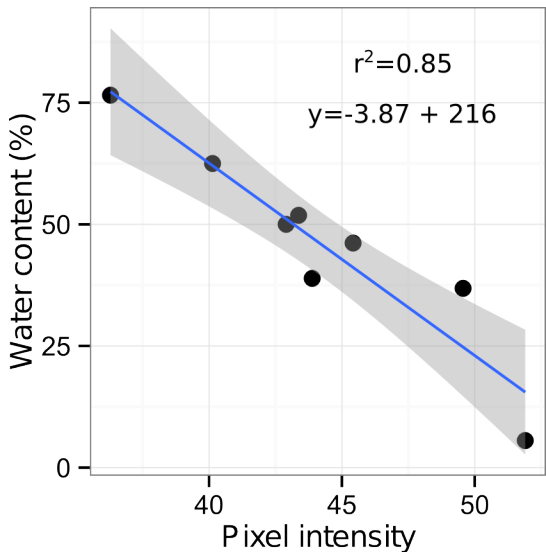
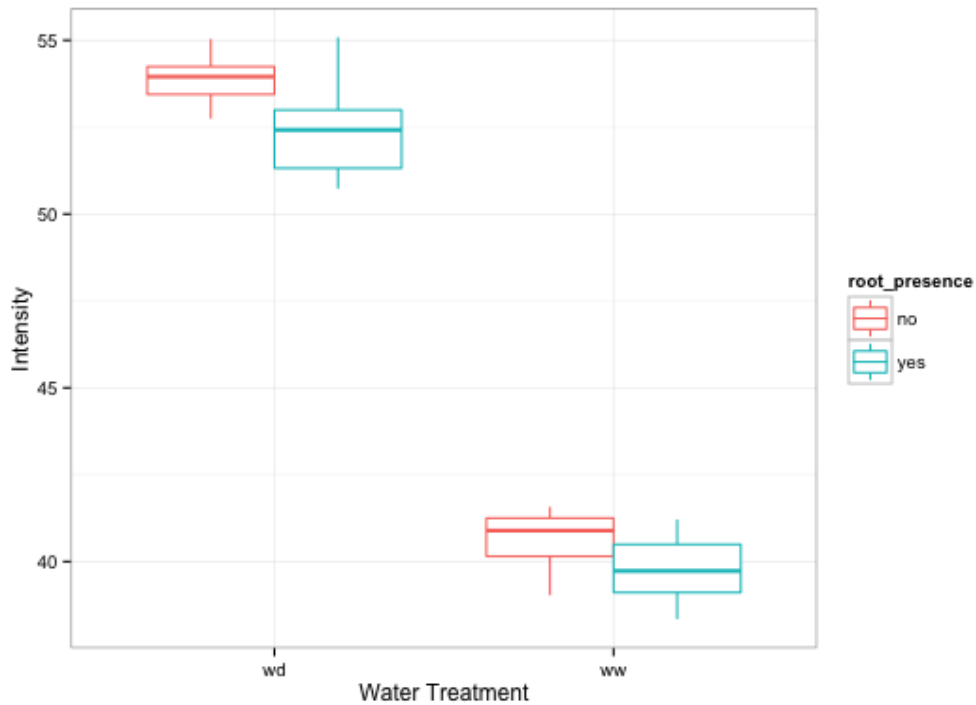


Figure 10—Supplement 6-figure

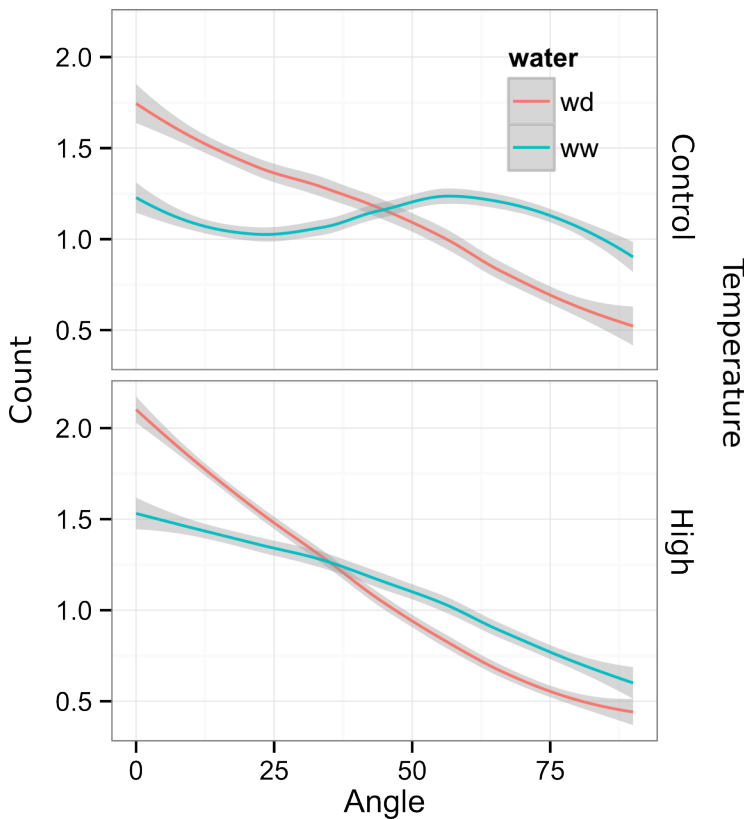
1107

1108 **supplement 1:** Moisture calibration curve. Rhizotrons with different levels of
 1109 moisture were prepared and scanned to obtain readings of pixel intensity. Soil from
 1110 rhizotrons was then weighed, dried down in an oven at 70 °C for 48 hours and percent water
 1111 content quantified.

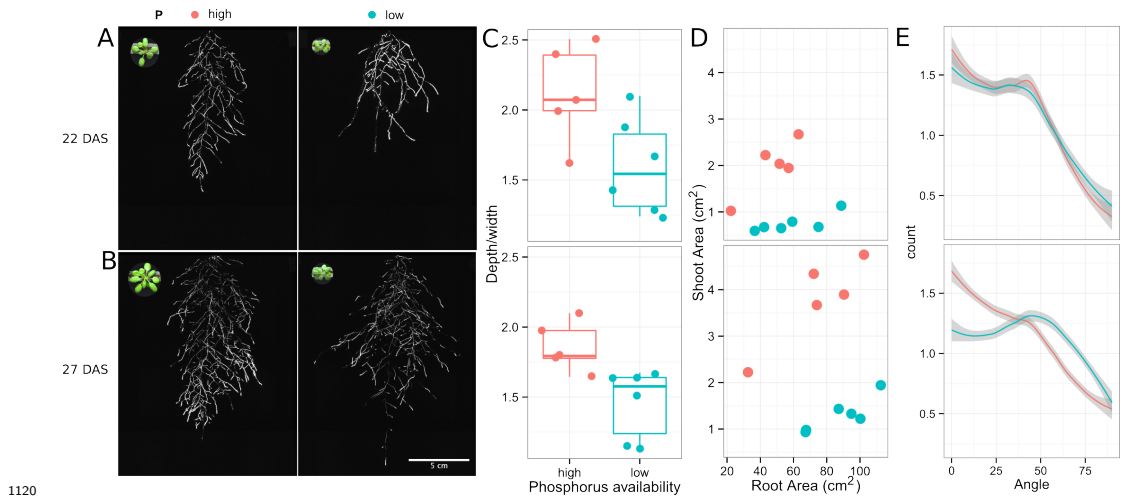


1112

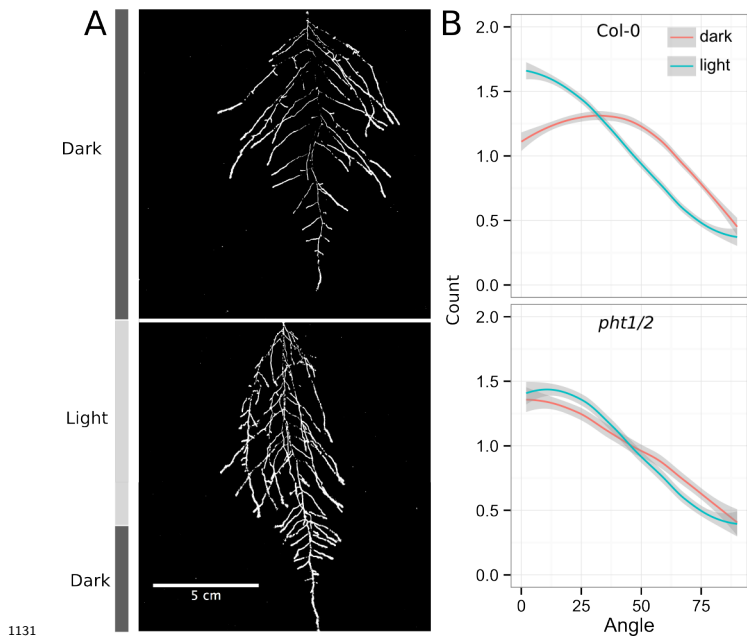
1113 **Figure 11-Supplement 16-figure supplement 2:** Comparison of soil intensity values
1114 between areas of the rhizotron with or without root presence. Mean intensity values from
1115 100 x 100 pixel squares samples of both areas were obtained from 10 different rhizotrons.



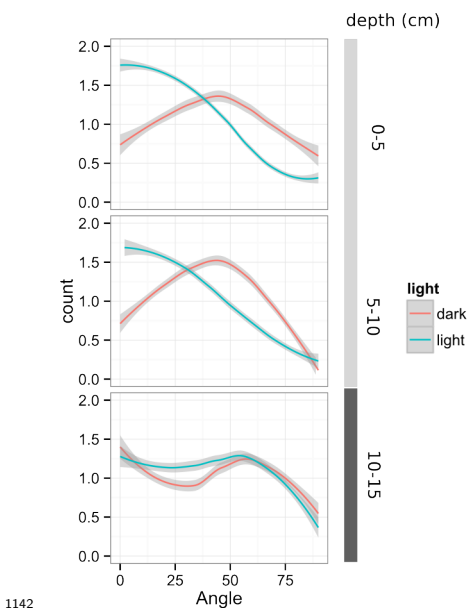
1116
1117 **Figure 7-figure supplement 1** Directionality analysis of roots of plants transferred to
1118 water deprivation conditions after 9 DAS and kept 22 °C (control temperature) and 29 °C
1119 (high temperature) until 22 DAS. (0° is the direction of the gravity vector).



1121 **Figure 7-figure supplement 2** Shoot and root systems of *ProUBQ10:LUC2a* Col-0
 1122 plants growing in soil supplemented with 1ml of 100 μM P-Alumina (left) and 0-P-Alumina
 1123 (right) 22 (A) or 27 (B) DAS. C) Root depth/width ratio of 22 (top) and 27 (bottom)
 1124 DAS plants. D) Scatter-plot showing relationship between root and shoot system area at
 1125 22 (top) and 27 (bottom) DAS. E) Root directionality distribution in plants 22 (top) and
 1126 27 (bottom) DAS. Anova analysis at $p < 0.01$ was used to compare depth/width ratios in
 1127 P treatments. Kolmogorov-Smirnov test at $p < 0.001$ was used to compare directionality
 1128 distributions between the different treatments. A Local Polynomial Regression Fitting
 1129 with 95% confidence interval (grey) was used to represent the directionality distribution
 1130 curve. (0° is the direction of the gravity vector).

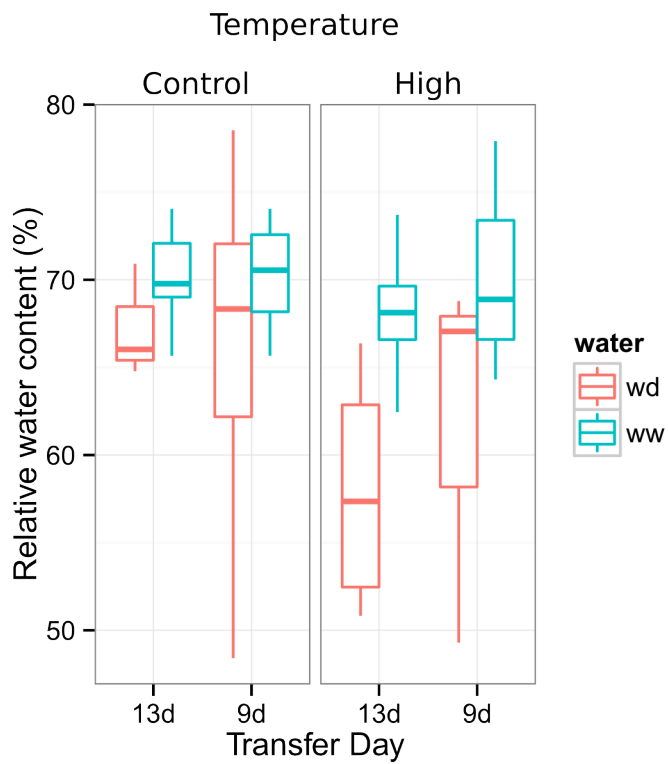


1132 **Figure 11-Supplement 27-figure supplement 3** A) Col-0 root systems shielded (top)
 1133 or light exposed (bottom). After 9 DAS the top third of the rhizotron was exposed to
 1134 light (indicated on the side with a light grey bar) and plants were imaged at 20 DAS. B)
 1135 Directionality analysis of root systems shielded (red) or exposed (green) to light for Col-0
 1136 (top panel) or *pht1/2* double mutant (bottom panel). Between 4 and 6 plants were analyzed
 1137 per treatment. ANOVA analysis at $p < 0.01$ was used to compare depth/width ratios in
 1138 P treatments. Kolmogorov-Smirnov test at $p < 0.001$ was used to compare directionality
 1139 distributions between the different treatments. A Local Polynomial Regression Fitting with
 1140 95% confidence interval (grey) was used to represent the directionality distribution curve. (0°
 1141 is the direction of the gravity vector).



1143 **Figure 7-figure supplement 4** Plots showing output of directionality analysis performed
1144 at different depths (0-5, 5-10, 10-15 cm) in rhizotrons exposed to light or kept in the dark.

1145 (0° is the direction of the gravity vector).



¹¹⁴⁷ **Figure 7-figure supplement 5** Leaf relative water content of 23 DAS plants that were
¹¹⁴⁸ subjected to water deprivation (ww) after 9 or 13 DAS or kept under well watered (ww)
¹¹⁴⁹ conditions. At 9 DAS half of the plants were kept under control temperature ~~conditions~~
¹¹⁵⁰ ~~conditions~~ (22 °C) and the other half transferred to a 29 °C (high) chamber. n = 6-8 plants.

¹¹⁵¹ **Supplemental Material 1**

¹¹⁵² Blueprints of the holders, clear sheets and spacers needed to built the rhizotrons. Additional
¹¹⁵³ details are provided in the materials and methods. Files are provided in Adobe Illustrator
¹¹⁵⁴ .ai and Autocad .dxf formats.

¹¹⁵⁵ **Supplemental Material 2**

¹¹⁵⁶ Primers used in the qPCR experiment.

¹¹⁵⁷ **Supplemental Material 3**

¹¹⁵⁸ Vector maps of all the constructs used in this work.

¹¹⁵⁹ **References**

- ¹¹⁶⁰ 1.Dinneny, J. R. *et al.* Cell identity mediates the response of *Arabidopsis* roots to abiotic
¹¹⁶¹ stress. *Science* **320**, 942–945 (2008).
- ¹¹⁶² 2.Duan, L. *et al.* Endodermal ABA Signaling Promotes Lateral Root Quiescence during Salt
¹¹⁶³ Stress in Arabidopsis Seedlings. *Plant Cell* **25**, 324–341 (2013).
- ¹¹⁶⁴ 3.Lynch, J. P. & Wojciechowski, T. Opportunities and challenges in the subsoil: pathways to
¹¹⁶⁵ deeper rooted crops. *J. Exp. Bot.* **66**, 2199–2210 (2015).
- ¹¹⁶⁶ 4.Brady, N. C. & Weil, R. R. *Elements of the nature and properties of soils*. (Prentice Hall,
¹¹⁶⁷ 2009).
- ¹¹⁶⁸ 5.Bao, Y. *et al.* Plant roots use a patterning mechanism to position lateral root branches
¹¹⁶⁹ toward available water. *Proc Natl Acad Sci* **111**, 9319–9324 (2014).
- ¹¹⁷⁰ 6.Tabata, R. *et al.* Perception of root-derived peptides by shoot LRR-RKs mediates systemic
¹¹⁷¹ N-demand signaling. *Science* **346**, 343–346 (2014).

- 1172 7. Marschner, P. *Marschner's Mineral Nutrition of Higher Plants*. (Academic Press, 2012).
1173 8. Rosquete, M. R. *et al.* An Auxin Transport Mechanism Restricts Positive Orthogravitropism
1174 in Lateral Roots. *Current Biology* **23**, 817–822 (2013).
1175 9. Uga, Y. *et al.* Control of root system architecture by DEEPER ROOTING 1 increases
1176 rice yield under drought conditions. *Nat. Genet.* **45**, 1097–1102 (2013).
1177 10. Postma, J. A. & Lynch, J. P. The optimal lateral root branching density for maize
1178 depends on nitrogen and phosphorus availability. *Plant Physiol.* **166**, 590–602 (2014).
1179 11. Kellermeier, F. *et al.* Analysis of the Root System Architecture of Arabidopsis Provides
1180 a Quantitative Readout of Crosstalk between Nutritional Signals. *The Plant Cell* **26**,
1181 1480–1496 (2014).
1182 12. Giehl, R. F., Lima, J. E., Wirén, N. von. Localized iron supply triggers lateral root
1183 elongation in arabidopsis by altering the AUX1-mediated auxin distribution. *Plant Cell* **24**,
1184 33–49 (2012).
1185 13. Galvan-Ampudia, C. S. *et al.* Halotropism Is a Response of Plant Roots to Avoid a Saline
1186 Environment. *Current Biology* **23**, 1–7 (2013).
1187 14. Geng, Y. *et al.* A spatio-temporal understanding of growth regulation during the salt
1188 stress response in Arabidopsis. *Plant Cell* **25**, 2132–2154 (2013).
1189 15. Slovak, R. *et al.* A Scalable Open-Source Pipeline for Large-Scale Root Phenotyping of
1190 Arabidopsis. *Plant Cell* **26**, 2390–2403 (2014).
1191 16. Moore, C. R. *et al.* High-throughput computer vision introduces the time axis to a
1192 quantitative trait map of a plant growth response. *Genetics* **195**, 1077–1086 (2013).
1193 17. Yokawa, K., Kagenishi, T., Baluška, F. Root photomorphogenesis in laboratory-maintained
1194 Arabidopsis seedlings. *Trends Plant Sci.* **18**, 117–119 (2013).
1195 18. Bueksch, A. *et al.* Image-based high-throughput field phenotyping of crop roots. *Plant
1196 Physiol.* **166**, 470–486 (2014).

- 1197 19.Trachsel, S., Kaeppeler, S. M., Brown, K. M. Lynch, J. P. Shovelomics: high throughput
1198 phenotyping of maize (*Zea mays* L.) root architecture in the field. *Plant Soil* **341**, 75–87
1199 (2011).–
- 1200 20.Devienne-Barret, F., Richard-Molard, C., Chelle, M., Maury, O. Ney, B. Ara-Rhizotron:
1201 an effective culture system to study simultaneously root and shoot development of
1202 *Arabidopsis*. *Plant Soil* **280**, 253–266 (2006).–
- 1203 21.Tracy, S. R. *et al.* Quantifying the impact of soil compaction on root system architecture
1204 in tomato (*Solanum lycopersicum*) by X-ray micro-computed tomography. *Annals of Botany*
1205 **110**, 511–519 (2012).–
- 1206 22.Grunewald, W. *et al.* Transcription factor WRKY23 assists auxin distribution patterns
1207 during *Arabidopsis* root development through local control on flavonol biosynthesis. *Proc
1208 Natl Acad Sci* **109**, 1554–1559 (2012).–
- 1209 23.10Hara-Miyauchi, C. *et al.* Bioluminescent system for dynamic imaging of cell and animal
1210 behavior. *Biochem. Biophys. Res. Commun.* **419**, 188–193 (2012).
- 1211 24.11Emami, S., Yee, M.-C. & Dinneny, J. R. A robust family of Golden Gate Agrobacterium
1212 vectors for plant synthetic biology. *Front. Plant Sc.* **4**, 339 (2013).–
- 1213 25.Lindeboom, J. J. 12Lobet, G. *et al.* A Mechanism for Reorientation of Cortical
1214 Microtubule Arrays Driven by Microtubule Severing. *Science* **342**, 1245533–1245533
1215 (2013).–
- 1216 26.Meijon, M., Satbhai, S. B., Tsuchimatsu, T. Busch, W. Genome-wide association study
1217 using cellular traits identifies a new regulator of root development in Root System Markup
1218 Language: toward a unified root architecture description language. *Nat Plant Physiol. Genet.*
1219 **46**167, 77–81 (2013)617–627 (2015).
- 1220 27.13Pacheco-Villalobos, D. & Hardtke, C. S. Natural genetic variation of root system
1221 architecture from *Arabidopsis* to *Brachypodium*: towards adaptive value. *Philosophical
1222 Transactions of the Royal Society of London B: Biological Sciences* **367**, 1552–1558 (2012).
- 1223 28.14Watt, M., Schneebeeli, K., Dong, P. & Wilson, I. W. The shoot and root growth of

- 1224 Brachypodium and its potential as a model for wheat and other cereal crops. *Functional*
1225 *Plant Biol.* **36**, 960–969 (2009).
- 1226 **29.15.** Mann, D. G. J. *et al.* Gateway-compatible vectors for high-throughput gene functional
1227 analysis in switchgrass (*Panicum virgatum L.*) and other monocot species. *Plant Biotechnol.*
1228 *J.* **10**, 226–236 (2012).
- 1229 **30.16.** Pacheco-Villalobos, D., Sankar, M., Ljung, K. & Hardtke, C. S. Disturbed Local Auxin
1230 Homeostasis Enhances Cellular Anisotropy and Reveals Alternative Wiring of Auxin-ethylene
1231 Crosstalk in Brachypodium distachyon Seminal Roots. *PLoS Genet* **9**, e1003564 (2013).
- 1232 **31.** Fang, S. *et al.* Genotypic recognition and spatial responses by rice roots. *Proc Natl Acad*
1233 *Sci* **110**, 2670–2675 (2013).
- 1234 **32.** Haney, C. H., Samuel, B. S., Bush, J. 17. Buer, C. S., Wasteneys, G. O. & Ausubel, F. M.
1235 ~~Associations with rhizosphere bacteria can confer an adaptive advantage to plants.~~ Masle,
1236 ~~J.~~ Ethylene modulates root-wave responses in *Arabidopsis*. *Nature Plants Plant physiology*
1237 **15051** (2015). doi:[132](https://doi.org/10.1038/nplants.2015.51), 1085–1096 (2003).
- 1238 **33.18.** Moreno-Risueno, M. A. *et al.* Oscillating gene expression determines competence for
1239 periodic *Arabidopsis* root branching. *Science* **329**, 1306–1311 (2010).
- 1240 **34.19.** Miller, G. *et al.* The plant NADPH oxidase RBOHD mediates rapid systemic signaling
1241 in response to diverse stimuli. *Science Signaling* **2**, ra45 (2009).
- 1242 **35.** Lynch, J., Brown, K. 20. Haney, C. H., Samuel, B. S., Bush, J. & Snyder, R. Controlled
1243 release fertilizer comprising modified alumina having phosphorous bound to alumina surface.
1244 (2001). at ⇔ Ausubel, F. M. ~~Associations with rhizosphere bacteria can confer an adaptive~~
1245 ~~advantage to plants.~~ *Nature Plants* **15051** (2015). doi:[10.1038/nplants.2015.51](https://doi.org/10.1038/nplants.2015.51)
- 1246 **36.21.** Mandoli, D. F., FORD, G. A., WALDRON, L. J., NEMSON, J. A. & Briggs, W. R.
1247 Some spectral properties of several soil types: implications for photomorphogenesis*. *Plant*
1248 *Cell Environ.* **13**, 287–294 (1990).
- 1249 **37.22.** Galen, C., Rabenold, J. J. & Liscum, E. Functional ecology of a blue light photoreceptor:
1250 effects of phototropin-1 on root growth enhance drought tolerance in *Arabidopsis thaliana*.

- 1251 *New Phytol.* **173**, 91–99 (2007).
- 1252 **38.23.** Moni, A., Lee, A. Y., Briggs, W. R. & Han, I. S. The blue light receptor Phototropin 1
1253 suppresses lateral root growth by controlling cell elongation. *Plant Biology* 34–40 (2014).
- 1254 **39.24.** Yokawa, K., Kagenishi, T. & Baluška, F. Root photomorphogenesis in laboratory-maintained
1255 *Arabidopsis* seedlings. *Trends Plant Sci.* **18**, 117–119 (2013).
- 1256 **25.** Lobell, D. B. *et al.* Greater Sensitivity to Drought Accompanies Maize Yield Increase in
1257 the U.S. Midwest. *Science* **344**, 516–519 (2014).
- 1258 **40.26.** Ort, D. R. & Long, S. P. Limits on Yields in the Corn Belt. *Science* **344**, 484–485
1259 (2014).
- 1260 **41.27.** Blossfeld, S., Schreiber, C. M., Liebsch, G., Kuhn, A. J. & Hinsinger, P. Quantitative
1261 imaging of rhizosphere pH and CO₂ dynamics with planar optodes. *Annals of Botany* **112**,
1262 267–276 (2013).
- 1263 **42.28.** Shaw, S. L. & Ehrhardt, D. W. Smaller, Faster, Brighter: Advances in Optical Imaging
1264 of Living Plant Cells. <http://dx.doi.org/10.1146/annurev-arplant-042110-103843> **64**, 351–375
1265 (2013).
- 1266 **43.** López-Arredondo, D. L., Leyva-González, M. A., González-Morales, S. I., López-Bueio,
1267 J. Herrera-Estrella, L. Phosphate Nutrition: Improving Low Phosphate Tolerance in Crops.
1268 *Annu. Rev. Plant Biol.* **65**, 95–123 (2014).—
- 1269 **44.** Lynch, J. P. Root phenes for enhanced soil exploration and phosphorus acquisition: tools
1270 for future crops. *Plant Physiol.* **156**, 1041–1049 (2011).—
- 1271 **45.29.** Grapov, D. DeviumWeb: Dynamic Multivariate Data Analysis and Visualization
1272 Platform.
- 1273 **46.30.** Branchini, B. R. *et al.* Red-emitting luciferases for bioluminescence reporter and
1274 imaging applications. *Analytical Biochemistry* **396**, 290–297 (2010).
- 1275 **47.31.** Branchini, B. R. *et al.* Thermostable red and green light-producing firefly luciferase
1276 mutants for bioluminescent reporter applications. *Analytical Biochemistry* **361**, 253–262

1277 (2007).

1278 48.32 Hall, M. P. *et al.* Engineered Luciferase Reporter from a Deep Sea Shrimp Utilizing a

1279 Novel Imidazopyrazinone Substrate. *ACS Chem. Biol.* **7**, 1848–1857 (2012).

1280 49.33 Lane, M. C., Alteri, C. J., Smith, S. N. & Mobley, H. L. T. Expression of flagella is

1281 coincident with uropathogenic Escherichia coli ascension to the upper urinary tract. *Proc.*

1282 *Natl. Acad. Sci. U.S.A.* **104**, 16669–16674 (2007).

1283 50.34 Ruegger, M. *et al.* The TIR1 protein of Arabidopsis functions in auxin response and is

1284 related to human SKP2 and yeast grr1p. *Genes Dev* **12**, 198–207 (1998).

1285 51.35 Moriwaki, T. *et al.* Hormonal Regulation of Lateral Root Development in Arabidopsis

1286 Modulated by MIZ1 and Requirement of GNOM Activity for MIZ1 Function. *Plant Physiol.*

1287 **157**, 1209–1220 (2011).

1288 52.36 Vogel, J. & Hill, T. High-efficiency Agrobacterium-mediated transformation of Brachy-

1289 podium distachyon inbred line Bd21-3. *Plant Cell Rep* **27**, 471–478 (2008).

1290 53.37 Covington, M. F. & Harmer, S. L. The Circadian Clock Regulates Auxin Signaling

1291 and Responses in Arabidopsis. *Plos Biol* **5**, e222 (2007).

1292 54.38 Lindeboom, J. J. *et al.* Root System Markup Language: toward a

1293 unified root architecture description language. A Mechanism for Reorientation of Cortical

1294 Microtubule Arrays Driven by Microtubule Severing. *Plant Physiol. Science* **167** 342,

1295 617–627 (2015) 1245533–1245533 (2013).

1296 55.39 R Core Team. *R: A language and environment for statistical computing*. (R Foundation

1297 for Statistical Computing, 2014). at <<http://www.R-project.org/>>

1298 56.40 Wickham, H. *Tidyr: Easily tidy data with spread() and gather() functions*. (2014). at

1299 <<http://CRAN.R-project.org/package=tidyr>>

1300 57.41 Auguie, B. *GridExtra: Functions in grid graphics*. (2012). at <<http://CRAN.R-project.org/package=gridExtra>>

- 1302 58.42.Dryden, I. L. *Shapes: Statistical shape analysis.* (2013). at <<http://CRAN.R-project.org/package=shapes>>
- 1303
- 1304 43.Adams, D. & Otarola-Castillo, E. Geomorph: An r package for the collection and analysis
1305 of geometric morphometric shape data. *Methods in Ecology and Evolution* **4**, 393–399 (2013).
- 1306
- 1307 44.Wickham, H. *Ggplot2: Elegant graphics for data analysis.* (Springer New York, 2009). at
1308 <<http://had.co.nz/ggplot2/book>>